Interpretability by Design for Efficient Multi-Objective Reinforcement Learning

Qiyue Xia [1 2] **Tianwei Wang** [2 3] **Michael Herrmann** [1 2]

Abstract

Multi-objective reinforcement learning (MORL) aims at optimising several, often conflicting goals to improve the flexibility and reliability of RL in practical tasks. This is typically achieved by finding a set of diverse, non-dominated policies that form a Pareto front in the performance space. We introduce LLE-MORL, an approach that achieves interpretability by design by utilising a training scheme based on the local relationship between the parameter space and the performance space. By exploiting a locally linear map between these spaces, our method provides an interpretation of policy parameters in terms of the objectives, and this structured representation enables an efficient search within contiguous solution domains, allowing for the rapid generation of high-quality solutions without extensive retraining. Experiments across diverse continuous control domains demonstrate that LLE-MORL consistently achieves higher Pareto front quality and efficiency than state-of-the-art approaches.

1. Introduction

Reinforcement Learning (RL) has shown great promise in complex decision-making problems, enabling significant advancements in a wide range (Silver et al., 2016; Levine et al., 2016). In real-world scenarios, however, problems often feature multiple, often conflicting, objectives. Under this circumstance, multi-objective approaches provide flexibility in practical applications of reinforcement learning by providing a modifiable policy that can be adjusted according to changes of preference among a set of objectives (Roijers et al., 2013; Hayes et al., 2022). This has fostered the development of the field known as multi-objective reinforcement learning (MORL). Ideally, the modifiable policies developed within MORL allow for efficient adaptation, ensuring that

a policy optimal for one set of preferences can be readily transformed to be optimal for a new set when those preferences change. To prepare such a modifiable policy for application, three problems have to be solved: (i) The *learning* problem involves the solution of an RL problem for each combination of preference parameters or at least for a representative subset of preferences. (ii) The *representation* problem requires a parametrization of the policies, which typically results in either a discrete set of individual policies (common in population-based methods) or a single, continuously adaptable policy (prevalent in deep reinforcement learning approaches). (iii) The *selection* problem is to identify a suitable policy in the application which includes dynamic adjustments to preference drifts and possibly the decision whether a different policy should be invoked or whether further training is required to respond to a temporary detection of suboptimality.

We propose to consider these problems as a coherent task, in order to reduce the computational burden of the learning problem and improve the interpretability of the policy representation. We hypothesise that if a continuous representation of policies can be found where similar preferences correspond to similar policy parameters, then small performance differences might be compensable with brief, targeted retraining. It is also anticipated that such a structured and interpretable policy representation would benefit the selection problem, though this aspect is not the primary focus of our current study.

While a globally continuous mapping is an ideal, we notice that in non-trivial problems, the relationship between the performance space and parameter space of policies is not a simple, single continuous mapping but can be described by a family of locally continuous components (Xu et al., 2020; Li et al., 2024). Our findings suggest that effectively exploring just a few of these components can be sufficient to achieve competitive performance in typical benchmark problems. To explore these components, we take a different perspective. Rather than searching for Pareto-optimal policies independently, we aim to trace the Pareto front manifold directly by exploring local structure in the high-dimensional policy parameter space. We formalise the Parameter-Performance Relationship (PPR), which captures the local correspondence between policy parameters and objective performance. This viewpoint enables an effi-

cient strategy for Pareto front (see Sect. 2.2) approximation: starting from a small set of policies, we can expand along directions that preserve PPR and generate new candidate solutions via a training-free extension stage, establishing an explicit and interpretable relationship between the policy parameter space and the reward space.

Based on this perspective, we develop a novel algorithm LLE-MORL (Locally Linear Extrapolation for Multi-Objective Reinforcement Learning). Our experiments demonstrate that the proposed algorithm can achieve high-quality Pareto front approximations with notable sample efficiency compared to existing approaches. By focusing on local structure in the policy parameter space, LLE-MORL reduces the need for exhaustive training while maintaining strong coverage and solution quality. Beyond efficiency, the structured use of the PPR provides an interpretable representation of the policy set, supporting a clearer understanding of local trade-offs along the Pareto front.

2. Background

2.1. Multi-Objective Reinforcement Learning

Multi-Objective Reinforcement Learning (MORL) extends the traditional RL framework to scenarios where agents must consider multiple, often conflicting objectives. This extension allows for more sophisticated decision-making models that mirror real-world complexities where trade-offs between competing goals, such as cost versus quality or speed versus safety, are common. To ground this notion formally, we represent a MORL problem as a Multi-Objective Markov Decision Process (MOMDP) which generalises the standard MDP framework to accommodate multiple reward functions, each corresponding to a different objective.

Definition 2.1. Multi-Objective Markov Decision Process (MOMDP). A MOMDP is defined by the tuple $(\mathcal{S}, \mathcal{A}, P, R, \gamma)$, where $\mathcal{S}$ is the state space, $\mathcal{A}$ is the action space, $P(s'|s, a)$ is the state transition probability, $R : \mathcal{S} \times \mathcal{A} \rightarrow \mathbb{R}^d$ is a vector-valued reward function with d as the number of objectives, specifying the immediate reward for each of the objectives, γ is the discount factor.

The crucial difference between MOMDPs and traditional single-objective MDPs is the reward structure. While single-objective MDPs use a scalar reward function, MOMDPs feature a vector-valued reward function that outputs d-dim vector rewards $\mathbf{r} = R(s, a)$, which delivers distinct numeric feedback for each objective. We denote a policy by π. At each timestep t, the agent in state $s_t \in \mathcal{S}$ selects an action $a_t \sim \pi(\cdot \mid s_t)$, transitions to a new state s_{t+1} with probability $P(s_{t+1} \mid s_t, a_t)$, and receives a reward vector $\mathbf{r}_t = \left[(R_1(s_t, a_t), R_2(s_t, a_t), \ldots, R_d(s_t, a_t)] \right)$. We define the discounted return vector by $\mathbf{G}_t = \sum_{k=0}^{\infty} \gamma^k \mathbf{r}_{t+k}$, and the multi-objective action-value function of a policy π

for a given state-action pair (s, a) by $\mathbf{Q}^\pi(s, a) = \mathbb{E}_\pi \big[\mathbf{G}_t \mid s_t = s, a_t = a \big]$. The goal of MORL is to find a policy π such that the expected return of each objective can be optimised. In practice, we trade off objectives via a scalarisation function $f_{\boldsymbol{\omega}}(\mathbf{r})$, which produces a scalar utility using preference vector $\boldsymbol{\omega} \in \Omega$, where Ω is the preferences space. The scalarisation function $f_{\boldsymbol{\omega}}(\mathbf{r})$ is used for mapping the multi-objective reward vector $\mathbf{r}(s, a)$ to a single scalar. In this paper, we consider the linear scalarisation function $f_{\boldsymbol{\omega}}(\mathbf{r}(s, a)) = \boldsymbol{\omega}^{\mathbf{T}} \mathbf{r}(s, a)$, where the preference vector $\boldsymbol{\omega}$ lies in the probability simplex, i.e., $\sum_{i=1}^{d} \omega_i = 1$ and $\omega_i \geq 0$, which is commonly used in MORL literature (Yang et al., 2019; Felten et al., 2024). When the preference dimension $d = 1$, the MOMDP reduces to a standard single-objective MDP under this linear scalarisation setting.

2.2. Pareto Optimality

In multi-objective optimisation, the concept of optimality differs from the single-objective case. Typically, no single policy simultaneously maximises all objectives, due to inherent trade-offs. Without any additional information about the user's preference, there can now be multiple possibly optimal solutions. In the following, we introduce several useful definitions for possibly optimal policies.

Definition 2.2. Pareto optimality. A policy π is said to *dominate* another policy π' if and only if $\forall i \in \{1, \ldots, d\}$, $V_i^\pi(s) \geq V_i^{\pi'}(s)$, and $\exists j, V_j^\pi(s) > V_j^{\pi'}(s)$, where $V_i^\pi(s) = \mathbb{E}_\pi[\sum_{t=0}^{\infty} \gamma^t R_i(s_t, a_t) \mid s_0 = s]$ denotes the expected discounted return for objective i under policy π. A policy π^* is *Pareto optimal* if and only if it is not dominated by another policy. The set of all Pareto optimal policies forms the *Pareto set*: $\Pi_P = \{\pi \mid \pi \text{ is Pareto optimal}\}$. The corresponding set of expected returns incured by policies in the Pareto set is termed *Pareto front*: $\mathcal{P} = \{V^\pi(s) \mid \pi \in \Pi_P\}$.

Since obtaining the true Pareto set is intractable in complex problems, the practical aim of multi-objective optimisation is to construct a finite set of policies that closely approximate the true Pareto front. So that practitioners can select the policy based on their preferred trade-off among objectives.

3. Methods

3.1. Parameter-Performance Relationship

Recent work in MORL has implicitly suggested a relationship between the parameter space of the policy network and the Pareto front in the performance space. (Xu et al., 2020) empirically show for PGMORL that each disjoint policy family occupies a continuous region in parameter space and maps to a contiguous segment of the Pareto front, while MORL/D (Felten et al., 2024) assume that policies with
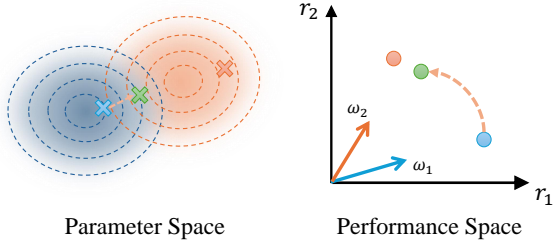
Figure 1. Parameter space and performance space of the Pareto policies. (Left) 2D projection of the high-dimensional policy parameter space. Red and blue gradient shadings and contour lines depict the scalarised reward under different preference vectors ω_1 and ω_2. The arrow marks a short retraining update. (Right) The policy obtained by retraining the θ_{w_1} model under ω_2 (green) shifts towards the new preference as seen in performance space.

similar parameters should lead to close evaluations. Motivated by these implicit observations, we introduce the a *parameter–performance relationship* and proceed to explain and empirically validate this property.

Definition 3.1. Parameter-Performance Relationship (PPR). Let $\Theta \subseteq \mathbb{R}^n$ be the space of policy parameters, and V be the expected discounted return as a function $V : \Theta \to \mathbb{R}^d$ of the parameter θ. We say that V exhibits a *parameter–performance relationship* on an open region $U \subseteq \Theta$ if $\exists \delta > 0$ and a function $h : U \times B_\delta(0) \to \mathbb{R}^d$, *s.t.* $\forall \theta \in U$ and perturbation $\Delta\theta$ satisfying $\|\Delta\theta\| < \delta$ and $\theta + \Delta\theta \in U$, the difference in the performance space is:

$$V(\theta + \Delta\theta) \ - \ V(\theta) \ = \ h\big(\theta, \Delta\theta\big). \tag{1}$$

where $B_\delta(0)$ is an open ball with radius δ centres on the origin, i.e. $B_\delta(0) := \{x : \|x\| < \delta\}$.

PPR is a local property and need not hold globally across the entire parameter space. In high-dimensional parameter spaces, policies with similar performance may be far apart in parameter space. This raises the question of how to identify policies that satisfy the PPR locally. As a first step, we require a metric for policy closeness in parameter space. We adopt the Hungarian matching distance (Kuhn, 1955; Munkres, 1957) to measure model distance and thereby quantify structural similarity between policies. A formal definition of Hungarian matching distance is provided in Appendix C.3. This metric naturally handles the permutation invariance of hidden units (Goodfellow et al., 2016) and measures the smallest structural change needed to align one model to another: lower Hungarian distance indicates greater model similarity.

As illustrated in Figure 1, a short retraining of a policy under a nearby preference typically induces a small, structured update in parameter space that corresponds to a predictable

shift in the expected returns. This observation motivates our use of brief retraining as a practical means of obtaining locally related policies for which the PPR holds.

3.2. Sanity Check

To obtain an initial empirical understanding of the PPR, we compare independently trained policies with those obtained via brief retraining. We first train two policies to a stable stage using a multi-objective PPO-based (Schulman et al., 2017) algorithm with scalarization vectors w_1 and w_2, yielding model parameters θ_{w_1} and θ_{w_2}. Starting from θ_{w_1}, we then perform one short additional training step with w_2 to obtain $\theta_{w'}$. We qualitatively evaluated the similarity between these policies using neuron heat maps at both the policy and value network levels in Figure 2a, and quantitatively by computing the Hungarian matching distances between model pairs in Figure 2b. Their corresponding rewards are visualised in the two-objective performance space for the multi-objective SWIMMER problem in Figure 2c.
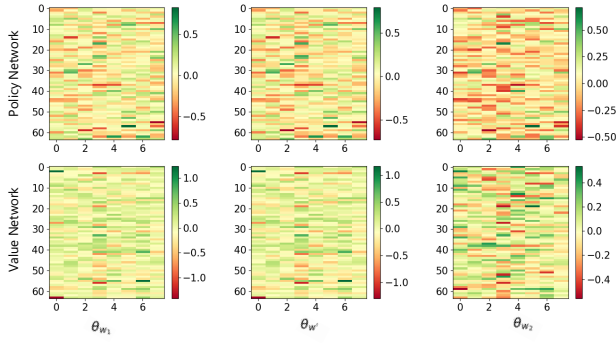
We compare three pairs of models: (1) θ_{w_1} and θ_{w_2}, representing independently trained policies that differ substantially in both parameter and performance space; (2) θ_{w_1} and $\theta_{w'}$, showing that brief retraining produces a structurally similar policy with a low Hungarian distance while inducing a clear shift in performance; and (3) $\theta_{w'}$ and θ_{w_2}, demonstrating that although their parameters remain distinct, their rewards lie much closer in the performance space.

These empirical observations indicate that a short retraining under a new preference produces a small, structured parameter update that directly maps to a predictable shift in performance, validating the PPR. More details of the sanity check procedure are provided in Appendix C.4.
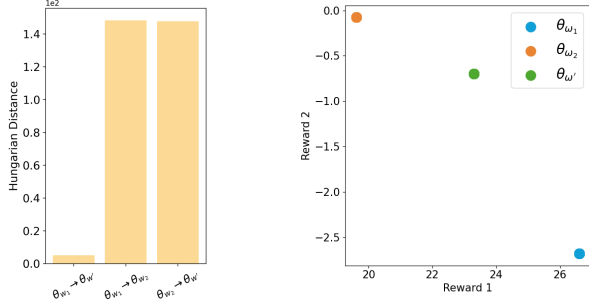
3.3. Locally Linear Extension

Based on the PPR definition, a natural question is whether the parameter-space difference between two policies that satisfy the PPR can serve as a directional update to extend an approximate Pareto front. To explore this, we consider two policies, a base policy θ_w and a retrained policy $\theta_{w'}$, which exhibit a PPR. Crucially, for this directional information to be meaningful for Pareto front exploration, both θ_w and $\theta_{w'}$ should ideally be non-dominated solutions, at least with respect to each other. Given such a pair, we compute the parameter update vector $\Delta\theta = \theta_{w'} - \theta_w$ and generate a set of intermediate policies by moving from the base policy θ_w along the parameter displacement $\Delta\theta$ in scaled steps. Concretely, for each scale α, we form $\theta_\alpha = \theta_w + \alpha\,\Delta\theta$ and evaluate its reward vectors in preference space.

Figure 3 visualises the resulting trajectory of reward vectors in the two-dimensional objective space: as α grows, the trajectory passes through the region around $\theta_{w'}$ and can extend

(a) Policy-net and value-net parameter heatmap. The horizontal axis corresponds to network layers, the vertical axis corresponds to neurons within each layer, and colour indicates the corresponding parameter values.

(b) Combined Hungarian model distance.

(c) Respective positions in performance space.

Figure 2. Comparing independently trained policy θ_{w_2} versus retrained policy $\theta_{w'}$ based on θ_{w_1}, for details see Section 3.2. The environment used here is the multi-objective SWIMMER problem.

beyond both the base and retrained endpoints, demonstrating how simple parameter-space moves can traverse broad trade-off regions, which offers a cost-effective strategy for efficiently expanding an approximate Pareto front without training each point from scratch.

3.4. The LLE-MORL Algorithm

Motivated by empirical observations, LLE-MORL is built on the hypothesis that there exists a manifold in parameter space that corresponds locally to the Pareto front and has the same intrinsic dimension, along which multi-objective performance varies smoothly. Theoretical analysis and formal proofs are provided in Section 3.5 and Appendix B.

Consider a d-objective MORL problem. The full Algorithm 1 (see Appendix A) consists of five stages: **(1) Initialisation:** We train a set of K base policies $\{\theta_{w_k}\}_{k=1}^{K}$ to convergence using PPO (Schulman et al., 2017). Each policy is trained under a distinct scalarization weight $w_k \in \Omega$, where these

weights are chosen to be evenly distributed across the preference space. **(2) Directional Retraining:** For each base policy $\theta_{w_k}(k = 1, \ldots, K)$, we estimate a set of $m = d - 1$ directions in parameter space by retraining. Specifically, for each $i = 1, \ldots, m$, we continue training from θ_{w_k} under a nearby preference $w_k^{(i)}$ for T_{dir} steps to obtain a directional policy $\theta_{w_k^{(i)}}$, where θ_{w_k} and $\theta_{w_k^{(i)}}$ are all non-dominated. We record $\Delta\theta_k^{(i)} = \theta_{w_k^{(i)}} - \theta_{w_k}$, and $\Delta w_k^{(i)} = w_k^{(i)} - w_k$ as the parameter update vector and the corresponding preference shift. **(3) Locally Linear Extension:** For each base policy θ_{w_k}, we generate candidate policies by extrapolating along the m local directions using $\{\Delta\theta_k^{(i)}\}_{i=1}^{m}$. Each candidate is constructed as a linear combination of these directions: $\theta_{k,\mathrm{cand}} = \theta_{w_k} + \sum_{i=1}^{m} \alpha_i \Delta\theta_k^{(i)}$, where step-scale factors α control the step sizes along each direction. We choose each α_i from a discrete grid defined by α_{start}, α_{end}, and step size $\Delta\alpha$, resulting in M possible values per direction. Iterating over all combinations across the m directions produces M^m candidate policies for each base solution. In parallel, we assign each candidate a matched preference weight $w_{k,\mathrm{cand}} = w_k + \sum_{i=1}^{m} \alpha_i \Delta w_k^{(i)}$. **(4) Candidate Selection:** All candidates $\theta_{k,\mathrm{cand}}$ generated in the locally linear extension stage are evaluated to obtain their respective performance vectors. We then select the subset of non-dominated candidates and forward them to the fine-tuning stage. **(5) Preference-Aligned Fine-Tuning:** For each selected candidate θ and its matched weight w, we perform a short PPO fine-tuning phase of T_{ref} steps under w to push the policy closer to the true Pareto front.

Together, these stages explore the local parameter-space structure, enabling efficient tracing of the local Pareto front manifold. This construction yields an interpretable policy representation: local directions in parameter space correspond to meaningful objective trade-offs, allowing parameter changes to be directly associated with movements along the Pareto front.

3.5. Theoretical Analysis

In this section, we present a theoretical analysis for the effectiveness of LLE-MORL, formally modelling the local manifold structure of Pareto-optimal policies and establishing guarantees for the locally linear extension mechanism used to trace the Pareto front. For clarity, we only provide the theory framework and its implications here, while consistent deductions and proofs are located in Appendix B.

First, the continuity of the reconstructed Pareto front by LLE-MORL is guaranteed by the Lipschitz continuity of PPR. Following Theorem 3.2 and Corollary 3.3 provide the theoretical foundation of these properties.

Theorem 3.2. *(Continuity of PPR function h.) Suppose that the expected discounted return V is defined by V :*

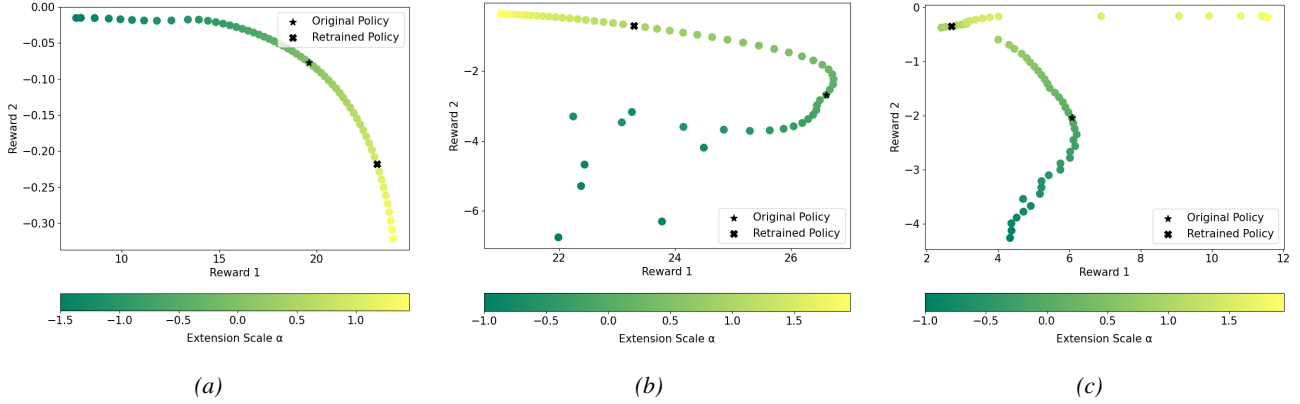*(a)*   *(b)*   *(c)*

Figure 3. Visualisation of the process of applying the parameter difference $\Delta\theta = \theta_{w'} - \theta_w$ between two related policies. The policies are obtained by first training a policy θ_w to a stable stage using scalarization vector w and then find policy $\theta_{w'}$ by a brief additional training period with a different scalarization vector w'. Iterating the shift $\Delta\theta$ in the policy space induces a sequence of shifts also in the multi-objective reward space. The subfigures show results for different initial preferences: (a) A convex front is found from the two policies. (b) Although the original policy turns out to be Pareto suboptimal, the solution manifold extends into a Pareto optimal component. (c) Retraining can cause the (Pareto-suboptimal) original solution to jump to a different branch so that the corresponding solution consists of two components one of which can be ignored because of Pareto suboptimality.

$U \to \mathbb{R}^d$, where $U \subseteq \Theta \subseteq \mathbb{R}^n$ is an open set. The sufficient condition for Lipschitz continuity of $h(\theta, \Delta\theta)$ with respect to the second variable $\Delta\theta$ is $V \in C^1(U)$ and $\forall a \in \mathcal{A}, s \in \mathcal{S}$

$$\sup_{\theta \in U} \left\| \nabla_\theta \log \pi_\theta(a|s) \right\| \leq \mathcal{G} < \infty, \qquad (2)$$

The inequality in Theorem 2 above states that the score function $\nabla_\theta \log \pi_\theta(a|s)$ (Baxter & Bartlett, 2001) is bounded by constant $\mathcal{G}$. This is a common assumption in related research (Aydin & Eksin, 2023; Shi et al., 2024).

Corollary 3.3. *(Surface continuity guaranteed by Lipschitz PPR) Algorithm LLE can construct a continuous surface in the performance space, as an approximation to Pareto front, given appropriate regularity conditions and range of α.*

Further, we aim to evaluate the error between the reconstructed result by LLE-MORL and the Pareto front $\mathcal{P}$. Assume $\mathcal{P}$ is a differentiable manifold of dimension m embedded in the Euclidean space of dimension d, i.e. $\mathcal{P} \in \mathcal{M}^m(\mathbb{R}^d)$, where $\dim\mathcal{P}$ is $m = d - 1$. Suppose the initialisation returns $\theta^{(0)}$, assuming it corresponds to a nondominated performance, where $v := V(\theta^{(0)}) \in \mathcal{P}$. Let $P_v \subset \mathcal{P}$ be an open neighbourhood of v on the manifold $\mathcal{P}$, where $P_v \in \mathcal{M}^m(\mathbb{R}^d)$. Define the neighbour of v to be P_v, assume there exists a parameter set $\Theta_v \subset \Theta$ bijectively mapping to P_v, denoted by $V|_{\Theta_v} : \Theta_v \to P_v$.

Theorem 3.4. *(Local lifting manifold) If both $V|_{\Theta_v}$ and $V|_{\Theta_v}^{-1}$ are C^k, i.e. $V|_{\Theta_v}$ is a diffeomorphism, then Θ_v is also a differentiable manifold embedded in $\mathbb{R}^n$ of the same dimension as P_v, i.e. $\Theta_v \in \mathcal{M}^m(\mathbb{R}^n)$.*

Therefore, the relation between Pareto front and corresponding parameters can be understand as the diffeomorphism

between two differentiable manifold of the same dimension m. Next, we define the expression of linear extension.

Condition 3.5. (Local extension directions) Suppose the directional retrain in LLE-MORL returns $\theta^{(i)} \in \Theta_v$, $i = 1, \dots, m$. Define

$$\mathcal{D} := \left[\theta^{(1)} - \theta^{(0)}, \ \dots, \ \theta^{(m)} - \theta^{(0)} \right] \in \mathbb{R}^{n \times m} \quad (3)$$

which has full column rank, i.e. $\mathrm{rank}(\mathcal{D}) = m$. Further, $\mathrm{span}(\mathcal{D})$ provides an approximation to the tangent space of Θ_v at $\theta^{(0)}$, i.e. $T_{\theta^{(0)}}\Theta_v$.

Theorem 3.6. *(Local Pareto error of LLE) Denote the local linear extrapolation by $\tilde{\theta}(\alpha) := \theta^{(0)} + \mathcal{D}\alpha$. Then, for a suitable range of $\alpha \in \mathbb{R}^m$, the error of extrapolation to the Pareto front is bounded, with first-order convergence as $\|\alpha\| \to 0$ and second-order increase as $\|\alpha\|$ grows.*

The explicit expression of error bound can be found in Equation 33 in Theorem B.13 in Appendix B. Theorem 3.6 support the effectiveness of LLE-MORL in constructing the Pareto front. And the error is controlled by an appropriate range of α, corresponding to the distance of linear extension. The empirical results and discussion is stated in Appendix D.2 for the feasibility of the choice of α.

4. Experiments

4.1. Experiment Setup

In this section, we evaluate the LLE-MORL algorithm using popular continuous MORL benchmark problems from the MO-Gymnasium-v5 (Felten et al., 2023). Our benchmark problems include three two-objective continuous environments: **MO-Swimmer**, **MO-Hopper-2d**, **MO-Ant-2d**, and
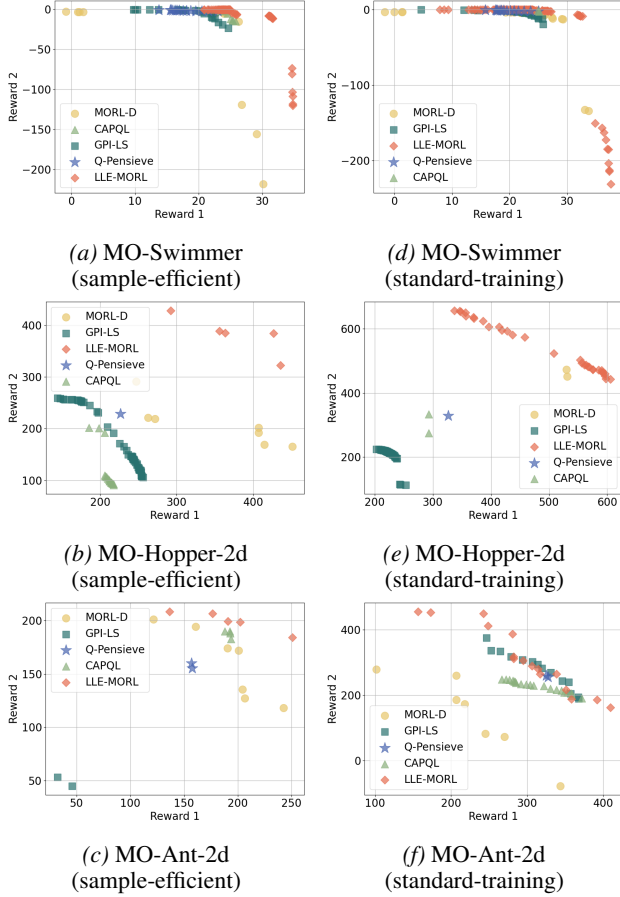
(a) MO-Swimmer
(sample-efficient)

(d) MO-Swimmer
(standard-training)

(b) MO-Hopper-2d
(sample-efficient)

(e) MO-Hopper-2d
(standard-training)

(c) MO-Ant-2d
(sample-efficient)

(f) MO-Ant-2d
(standard-training)

Figure 4. Pareto fronts from 2 different settings, comparing our LLE-MORL method with baselines on three 2d continuous-control benchmarks. LLE-MORL consistently achieves wider coverage and closer proximity to the true Pareto front.

two three-objective continuous environments: **MO-Hopper-3d**, **MO-Ant-3d**. We evaluate the quality of the approximate Pareto front using three standard metrics: **Hypervolume (HV)**, **Expected Utility (EU)**, **Sparsity (SP)**, following the formalism in (Zitzler & Thiele, 2002; Zintgraf et al., 2015; Hayes et al., 2022). Higher HV and EU values indicate better overall front quality, while SP measures the distribution of solutions along the front. Since SP is scale-dependent and less directly related to decision quality, we report it mainly as a complementary metric to assess coverage diversity. More details can be found in Appendix C.

We compare our LLE-MORL against the following state-of-the-art MORL algorithms: (i) **GPI-LS** (Alegre et al., 2023) applies Generalised Policy Improvement over a discretised set of preference weights and uses linear scalarization to construct a diverse Pareto set. (ii) Concave-augmented Pareto Q-learning (**CAPQL**) (Lu et al., 2023): learns an ensemble of Q-functions under different preferences and selects actions via conservative aggregation to improve front coverage. (iii) **Q-Pensieve** (Hung et al., 2023) boosts the sample

efficiency of MORL by storing past Q-function snapshots in a replay buffer, enabling explicit policy-level knowledge sharing across training iterations. (iv) **MORL/D** (Felten et al., 2024) is a deep-RL analogue of decomposition-based multi-objective optimisation that trains subpolicies under scalarised objectives and recombines them via weight decompositions to approximate the Pareto front.

4.2. Results and Analysis on 2D Benchmarks

To assess the performance of MORL, we now present quantitative results evaluating the quality of the approximated Pareto fronts on 2D-objective benchmarks. We conduct experiments under two distinct settings to provide a comprehensive understanding of these algorithms' capabilities: **(1) Sample-Efficient Setting:** All methods, including our LLE-MORL approach, were trained under an interaction budget for 1.5×10^5 timesteps (including all algorithmic training phases). Given the complexity of continuous control benchmarks, this relatively limited interaction budget serves as a critical testbed for evaluating how rapidly different MORL strategies can discover effective Pareto front approximations. **(2) Standard-Training Setting:** To assess performance under more common training conditions, most methods, including our LLE-MORL approach, under an interaction budget for 1×10^6 timesteps. This setting aligns with common practices for benchmarking in continuous control and allows us to assess the final quality of the Pareto fronts achieved by each algorithm after a more thorough learning process. In all experiments, we fix hyperparameters according to a common setting shared across methods, without assuming any task-specific parameter tuning. Full implementation details are provided in Appendix C.

In the sample-efficient setting, shown in Figure 4 left column and Table 1 top part, LLE-MORL achieves the highest HV and EU in all benchmarks, demonstrating strong capabilities in rapidly achieving high-quality Pareto fronts. Regarding SP, while LLE-MORL does not consistently achieve the leading scores on this metric, its performance generally reflects a good and effective distribution of solutions along the high-quality Pareto fronts it identifies. It should be noted that SP results can be confounded by a fragmentary recovery of the Pareto front. For instance, if Q-Pensieve discovers only two close points of the Pareto front for the MO-Ant problem, the sparsity rating is nearly perfect. Meanwhile, a low SP might also arise from solutions being overly clustered in a small region, as potentially seen with GPI-LS and Q-Pensieve in MO-Swimmer shown in Figure 4a.

Transitioning to the standard-training setting, shown in Figure 4 right column and Table 1 bottom part, across all benchmarks, LLE-MORL typically achieves the highest HV and highly competitive EU. This superior performance indicates that LLE-MORL finds a more extensive and higher-quality

Table 1. Evaluation of the quality of the Pareto front on 2D-objective benchmarks under different settings.

Setting	Environment	Metric	Method					
			GPI-LS	CAPQL	Q-Pensieve	MORL/D	LLE-MORL-0	LLE-MORL
Sample-efficient	MO-Swimmer	HV(10^4)	4.80±0.43	5.00±0.09	4.77±0.17	5.72±0.25	6.54±0.10	**6.77±0.17**
		EU(10^1)	0.89±0.14	1.08±0.01	1.06±0.11	1.00±0.01	0.93±0.11	**1.11±0.02**
		SP(10^2)	1.12±1.02	1.68±1.33	**0.82±0.61**	11.03±7.17	1.61±1.21	1.78±1.60
	MO-Hopper-2d	HV(10^5)	1.06±0.12	1.40±0.31	1.00±0.05	1.96±0.19	2.73±0.17	**3.02±0.28**
		EU(10^2)	2.11±0.17	2.68±0.40	2.16±0.08	3.29±0.15	4.15±0.20	**4.36±0.28**
		SP(10^2)	5.35±3.64	1.33±1.21	**0.08±0.04**	48.25±22.90	8.08±6.44	15.13±8.31
	MO-Ant-2d	HV(10^4)	3.24±1.28	8.10±0.64	5.01±1.73	9.73±0.42	10.07±0.63	**10.44±0.56**
		EU(10^2)	0.72±0.30	1.82±0.10	1.18±0.41	2.03±0.08	2.16±0.10	**2.23±0.08**
		SP(10^3)	1.14±1.01	**0.05±0.03**	0.12±0.10	1.33±1.02	1.51±0.36	1.22±0.22
Standard-training	MO-Swimmer	HV(10^4)	5.46±0.17	5.12±0.32	5.20±1.08	7.05±0.39	7.74±0.22	**7.82±0.24**
		EU(10^1)	1.06±0.03	1.10±0.05	1.13±0.15	1.13±0.03	1.03±0.07	**1.16±0.09**
		SP(10^2)	**0.04±0.02**	0.12±0.09	0.05±0.02	4.36±1.64	1.11±0.56	1.15±0.63
	MO-Hopper-2d	HV(10^5)	1.15±0.04	2.11±0.91	1.62±0.20	3.75±0.25	4.76±0.08	**4.87±0.09**
		EU(10^2)	2.26±0.07	3.46±1.07	2.76±0.84	4.98±0.17	5.67±0.10	**5.74±0.07**
		SP(10^2)	0.95±0.73	15.37±10.67	**0.02±0.01**	10.60±6.31	5.09±1.77	4.53±1.79
	MO-Ant-2d	HV(10^5)	1.72±0.93	1.63±0.72	1.78±0.34	1.84±0.31	2.58±0.22	**2.68±0.22**
		EU(10^2)	2.68±1.19	2.81±0.80	2.18±0.41	3.09±0.30	3.81±0.27	**3.93±0.26**
		SP(10^3)	0.57±0.50	0.28±0.24	**0.10±0.09**	3.92±2.81	2.23±0.97	1.59±0.40

set of solutions, which strongly suggests a better approximation of the Pareto front compared to the baselines. The evidence from Pareto front visualisation further corroborates LLE-MORL's advantages. In the MO-Swimmer environment, shown in Figure 4d, LLE-MORL more comprehensively explores the objective space, successfully identifying Pareto optimal solutions in the lower-right region consistently missed by baselines such as GPI-LS, Q-Pensieve and CAPQL. Notably, when comparing the GPI-LS, CAPQL and Q-Pensieve performance to those in the sample-efficient setting for the MO-Swimmer environment, these particular baselines appear to remain constrained by suboptimal solutions in this challenging region, indicating that simply extending training duration did not resolve their exploration deficiencies here. While LLE-MORL's thorough exploration to achieve this broader coverage means its SP may not be the numerically lowest, the result could be well-justified by the extensive nature of the front.

In summary, LLE-MORL consistently achieves high-quality Pareto fronts across different settings. Its innovative training-free extension step enables efficient generation of diverse solutions, yielding strong performance under limited budgets and consistently improved results with extended training. Runtime comparisons are reported in Appendix C.

4.3. Performance and Scalability in Higher Dimensional Objective Spaces

To evaluate the robustness and discuss the scalability of LLE-MORL beyond standard 2D-objective trade-offs, we extended our experimental evaluation to higher-dimensional scenarios using the MO-Hopper-3d and MO-Ant-3d benchmarks. In these environments, the Pareto front is no longer a one-dimensional curve but a two-dimensional manifold embedded in a three-dimensional performance space. All methods, including our LLE-MORL approach, were trained under an interaction budget for 2×10^6 timesteps (including all algorithmic training phases).

The experimental results, reported in Table 2, are highly consistent with the observations from our 2D benchmarks, showing that LLE-MORL maintains a significant advantage in HV and EU over baselines. The robust performance in higher dimensions is a direct consequence of the algorithm's design, which generalises to d-objective tasks without requiring additional algorithmic modifications. As established in our theoretical analysis (Section 3.5), the $d-1$ directional vectors obtained during the retraining phase are sufficient to explore and span the local Pareto manifold. This allows the locally linear extension mechanism to fill in contiguous patches of the Pareto surface effectively.

4.4. Ablation Study

The LLE-MORL integrates a locally linear extension process with a subsequent fine-tuning stage. To understand the distinct contributions of these components to the overall performance, our ablation study separates them. We first evaluate LLE-MORL-0, which solely employs the extension process without fine-tuning. As detailed in Table 1 and Table 2, LLE-MORL-0 itself demonstrates competitiveness, achieving strong HV and EU scores that are often competitive with or superior to baselines. This emphasises the efficacy of our extension mechanism in rapidly discovering a high-quality approximation of the Pareto front.

Subsequently, we assess the improvement of the fine-tuning stage by comparing LLE-MORL (which includes fine-tuning) to LLE-MORL-0. This comparison reveals that the inclusion of fine-tuning yields further improvements in

Table 2. Evaluation of the quality of the Pareto front on 3D-objective benchmarks.

Environment	Metric	Method					
		GPI-LS	CAPQL	Q-Pensieve	MORL/D	LLE-MORL-0	LLE-MORL
MO-Hopper-3d	HV(10^7)	5.78±5.49	4.53±2.64	5.23±3.89	9.01±0.10	10.20±0.36	**10.63±0.40**
	EU(10^2)	1.63±0.11	2.51±0.79	2.49±0.88	3.82±0.06	3.58±0.35	**3.69±0.23**
	SP(10^2)	**0.23±0.09**	29.04±16.92	48.44±37.93	12.37±3.67	1.33±0.98	1.35±1.14
MO-Ant-3d	HV(10^7)	1.10±0.37	2.49±0.14	0.71±0.36	2.69±0.01	3.38±0.38	**3.61±0.31**
	EU(10^2)	1.31±0.38	1.90±0.03	1.09±0.25	1.98±0.04	1.89±0.14	**1.96±0.15**
	SP(10^2)	27.79±22.62	3.72±3.70	51.57±51.73	13.45±17.23	0.65±0.28	**0.54±0.15**

HV and EU across all settings. The impact on SP is less uniform, which is an expected outcome, as refining solutions towards a more optimal Pareto front can alter their relative spacing. Nevertheless, the consistent enhancements in HV and EU prove the value of fine-tuning for improving the quality of the approximate Pareto front and its coverage by diverse solutions. This demonstrates that the extension process provides a strong foundation for the fine-tuning stage that enables LLE-MORL to outperform other algorithms.

5. Related work

Prior work in MORL offers various strategies for handling conflicting objectives. These can be broadly grouped into single-policy methods and multi-policy methods for approximating the Pareto front. Single-policy approaches typically convert the multi-objective problem into a single-objective task using a predefined preference or weighting scheme. A common instance of such a weighting scheme is linear scalarization (Van Moffaert et al., 2013). Limitations of linear scalarization, particularly in capturing non-convex Pareto fronts, have been addressed by more advanced scalarization functions such as Chebyshev methods (Van Moffaert et al., 2013), hypervolume-based approaches (Zhang & Golovin, 2020) and the addition of concave terms to rewards (Lu et al., 2023). Concurrently, significant efforts have developed generalised single-policy models conditioned on preference inputs to achieve adaptability across diverse objectives (Teh et al., 2017; Yang et al., 2019; Basaklar et al., 2022; Parisi et al., 2016), with subsequent extensions into offline learning contexts (Zhu et al., 2023; Lin et al., 2024) and methods to improve sample efficiency in these settings (Hung et al., 2023).

Multi-policy MORL strategies directly target the approximation of the entire Pareto front by learning a diverse collection of policies. One direction is developing single models conditioned on preferences (Abels et al., 2019; Friedman & Fontaine, 2018; Kyriakis & Deshmukh, 2022). Other approaches explicitly learn a diverse set of policies or their value functions; this includes direct value-based methods like Pareto Q-learning (Van Moffaert & Nowé, 2014), and evolutionary algorithms often guided by prediction models to discover a dense Pareto front (Xu et al., 2020). Fur-

ther techniques for generating policy sets involve Generalised Policy Improvement (GPI) for sample-efficient learning (Alegre et al., 2023) or the development of transferable policy components using representations like successor features (Alegre et al., 2022). The use of constrained optimisation to efficiently complete and refine the Pareto front is also explored in (Liu et al., 2024; He et al., 2024). Furthermore, the principles of decomposition-based strategies, which find a set of solutions by solving multiple interrelated scalarised sub-problems, have been a significant focus (Felten et al., 2024; Röpke et al., 2024).

While these single-policy and multi-policy paradigms have significantly advanced MORL, the characterisation and systematic exploitation of the structural relationship between the learned policies' underlying parameter space and their resultant performance on the Pareto front remain largely underexplored. Although multi-objective optimisation offers techniques for Pareto navigation (Ye & Liu, 2022) and model merging (Rame et al., 2023; Chen & Kwok, 2025), and prior MORL studies have touched upon parameter space regularities (Xu et al., 2020), policy manifolds (Parisi et al., 2016; Shu et al., 2024), front geometries (Li et al., 2024), or preference control (Yuan et al., 2025; Yang et al., 2025), these directions do not provide a mechanism to systematically explore the local Pareto structure in a way that is interpretable and enables guided expansion.

6. Conclusion

We have discussed LLE-MORL, an algorithm that identifies solution components in multi-objective reinforcement learning by directed exploration of the Pareto front. The main benefit of LLE-MORL is interpretability and increased efficiency which is enabled by maintaining a direct relation between the multi-objective performance and the representation of the policy in the parameter space. We have shown that this simple set-up is sufficient to obtain a high-quality Pareto front from both empirical and theoretical aspects, and the LLE-MORL is superior to recent MORL algorithms. Furthermore, as the LLE stage is a modular plug-in component, it can be integrated into existing deep RL algorithms as a training-free and computationally lightweight module, offering a simple path for future extensions.

Acknowledgements

Impact Statement

This paper aims to advance the field of multi-objective reinforcement learning by proposing a more efficient and interpretable algorithmic framework for approximating Pareto fronts. MORL could provide a flexible approach for adapting policies to user needs when these can be expressed through combinations of evaluative signals. We have shown that it is possible to achieve such an approach with strikingly less computational effort than the direct solutions, thereby reducing energy consumption and required computing resources. Likewise, improved results can be achieved in a shorter time, which can open the route to new applications e.g. in online process optimisation or control of complex systems, and enables the optimisation of more criteria in existing problems. The intended impact of this work is methodological, aimed at supporting research in reinforcement learning and multi-objective optimisation. As a general-purpose learning approach, the societal impacts of the proposed method depend on its application domain and on any side effects; we do not foresee any negative consequences within its intended scope.

References

Abels, A., Roijers, D., Lenaerts, T., Nowé, A., and Steckelmacher, D. Dynamic weights in multi-objective deep reinforcement learning. In *International Conference on Machine Learning*, pp. 11–20. PMLR, 2019.

Alegre, L. N., Bazzan, A., and Da Silva, B. C. Optimistic linear support and successor features as a basis for optimal policy transfer. In *International Conference on Machine Learning*, pp. 394–413. PMLR, 2022.

Alegre, L. N., Bazzan, A. L., Roijers, D. M., Nowé, A., and da Silva, B. C. Sample-efficient multi-objective learning via generalized policy improvement prioritization. In *Proceedings of the 2023 International Conference on Autonomous Agents and Multiagent Systems*, pp. 2003–2012, 2023.

Aydin, S. and Eksin, C. Policy gradient play with networked agents in markov potential games. In Matni, N., Morari, M., and Pappas, G. J. (eds.), *Proceedings of The 5th Annual Learning for Dynamics and Control Conference*, volume 211 of *Proceedings of Machine Learning Research*, pp. 184–195. PMLR, 15–16 Jun 2023. URL https://proceedings.mlr.press/v211/aydin23a.html.

Basaklar, T., Gumussoy, S., and Ogras, U. PD-MORL: Preference-driven multi-objective reinforcement learning algorithm. *arXiv preprint arXiv:2208.07914*, 2022.

Baxter, J. and Bartlett, P. L. Infinite-horizon policy-gradient estimation. *Journal of Artificial Intelligence Research*, 15:319–350, 2001.

Chen, W. and Kwok, J. Pareto merging: Multi-objective optimization for preference-aware model merging. In *Forty-second International Conference on Machine Learning*, 2025. URL https://openreview.net/forum?id=D7qRwx6BOS.

Felten, F., Alegre, L. N., Nowé, A., Bazzan, A. L. C., Talbi, E. G., Danoy, G., and Silva, B. C. d. A toolkit for reliable benchmarking and research in multi-objective reinforcement learning. In *Advances in Neural Information Processing Systems*, volume 36, pp. 23671–23700, 2023.

Felten, F., Talbi, E.-G., and Danoy, G. Multi-objective reinforcement learning based on decomposition: A taxonomy and framework. *Journal of Artificial Intelligence Research*, 79:679–723, 2024.

Friedman, E. and Fontaine, F. Generalizing across multi-objective reward functions in deep reinforcement learning. *arXiv preprint arXiv:1809.06364*, 2018.

Goodfellow, I., Bengio, Y., and Courville, A. *Deep learning*. MIT Press, Cambridge, 2016.

Hayes, C. F., Rădulescu, R., Bargiacchi, E., Källström, J., Macfarlane, M., Reymond, M., Verstraeten, T., Zintgraf, L. M., Dazeley, R., Heintz, F., et al. A practical guide to multi-objective reinforcement learning and planning. *Autonomous Agents and Multi-Agent Systems*, 36(1):26, 2022.

He, X., Hu, Z., Yang, H., and Lv, C. Personalized robotic control via constrained multi-objective reinforcement learning. *Neurocomputing*, 565:126986, 2024.

Hung, W., Huang, B. K., Hsieh, P.-C., and Liu, X. Q-pensieve: Boosting sample efficiency of multi-objective RL through memory sharing of q-snapshots. In *The Eleventh International Conference on Learning Representations*, 2023. URL https://openreview.net/forum?id=AwWaBXLIJE.

Kuhn, H. W. The Hungarian method for the assignment problem. *Naval Research Logistics Quarterly*, 2(1-2): 83–97, 1955.

Kyriakis, P. and Deshmukh, J. Pareto policy adaptation. In *International Conference on Learning Representations*, volume 2022, 2022.

Levine, S., Finn, C., Darrell, T., and Abbeel, P. End-to-end training of deep visuomotor policies. *Journal of Machine Learning Research*, 17(39):1–40, 2016.

Li, Y., Ju, P., and Shroff, N. B. How to find the exact Pareto front for multi-objective MDPs? *arXiv preprint arXiv:2410.15557*, 2024.

Lin, Q., Yu, C., Liu, Z., and Wu, Z. Policy-regularized offline multi-objective reinforcement learning. In *AAMAS*, pp. 1201–1209, 2024. URL https://dl.acm.org/doi/10.5555/3635637.3662977.

Liu, R., Pan, Y., Xu, L., Song, L., You, P., Chen, Y., and Bian, J. C-MORL: Multi-objective reinforcement learning through efficient discovery of Pareto front. *arXiv preprint arXiv:2410.02236*, 2024.

Lu, H., Herman, D., and Yu, Y. Multi-objective reinforcement learning: Convexity, stationarity and Pareto optimality. In *The Eleventh International Conference on Learning Representations*, 2023.

Munkres, J. Algorithms for the assignment and transportation problems. *Journal of the Society for Industrial and Applied Mathematics*, 5(1):32–38, 1957.

Parisi, S., Pirotta, M., and Restelli, M. Multi-objective reinforcement learning through continuous Pareto manifold approximation. *Journal of Artificial Intelligence Research*, 57:187–227, 2016.

Raffin, A., Hill, A., Ernestus, M., Gleave, A., Kanervisto, A., and Dormann, N. PyTorch version of stable baselines. https://github.com/DLR-RM/stable-baselines3, 2019.

Rame, A., Couairon, G., Dancette, C., Gaya, J.-B., Shukor, M., Soulier, L., and Cord, M. Rewarded soups: towards pareto-optimal alignment by interpolating weights fine-tuned on diverse rewards. In Oh, A., Naumann, T., Globerson, A., Saenko, K., Hardt, M., and Levine, S. (eds.), *Advances in Neural Information Processing Systems*, volume 36, pp. 71095–71134. Curran Associates, Inc., 2023.

Roijers, D. M., Vamplew, P., Whiteson, S., and Dazeley, R. A survey of multi-objective sequential decision-making. *Journal of Artificial Intelligence Research*, 48:67–113, 2013.

Röpke, W., Reymond, M., Mannion, P., Roijers, D. M., Nowé, A., and Rădulescu, R. Divide and conquer: Provably unveiling the Pareto front with multi-objective reinforcement learning. *Preprint: arXiv:2402.07182*, 2024.

Schulman, J., Wolski, F., Dhariwal, P., Radford, A., and Klimov, O. Proximal policy optimization algorithms. *arXiv preprint arXiv:1707.06347*, 2017.

Shi, J., Wang, X., Zhang, M., Liu, M., Zhu, J., and Wu, Q. A distributed adaptive policy gradient method based on momentum for multi-agent reinforcement learning. *Complex & Intelligent Systems*, 10(5):7297–7310, 2024.

Shu, T., Shang, K., Gong, C., Nan, Y., and Ishibuchi, H. Learning pareto set for multi-objective continuous robot control. In *Proceedings of the Thirty-Third International Joint Conference on Artificial Intelligence*, IJCAI '24, 2024. ISBN 978-1-956792-04-1. doi: 10.24963/ijcai.2024/544. URL https://doi.org/10.24963/ijcai.2024/544.

Silver, D., Huang, A., Maddison, C. J., Guez, A., Sifre, L., Van Den Driessche, G., Schrittwieser, J., Antonoglou, I., Panneershelvam, V., Lanctot, M., et al. Mastering the game of Go with deep neural networks and tree search. *nature*, 529(7587):484–489, 2016.

Teh, Y., Bapst, V., Czarnecki, W. M., Quan, J., Kirkpatrick, J., Hadsell, R., Heess, N., and Pascanu, R. Distral: Robust multitask reinforcement learning. *Advances in Neural Information Processing Systems*, 30, 2017.

Vamplew, P., Yearwood, J., Dazeley, R., and Berry, A. On the limitations of scalarisation for multi-objective reinforcement learning of Pareto fronts. In *AI 2008: Advances in Artificial Intelligence: 21st Australasian Joint Conference on Artificial Intelligence Auckland, New Zealand, December 1-5, 2008. Proceedings 21*, pp. 372–378. Springer, 2008.

Van Moffaert, K. and Nowé, A. Multi-objective reinforcement learning using sets of Pareto dominating policies. *The Journal of Machine Learning Research*, 15(1):3483–3512, 2014.

Van Moffaert, K., Drugan, M. M., and Nowé, A. Scalarized multi-objective reinforcement learning: Novel design techniques. In *2013 IEEE symposium on adaptive dynamic programming and reinforcement learning (ADPRL)*, pp. 191–199. IEEE, 2013.

Xu, J., Tian, Y., Ma, P., Rus, D., Sueda, S., and Matusik, W. Prediction-guided multi-objective reinforcement learning for continuous robot control. In *International Conference on Machine Learning*, pp. 10607–10616. PMLR, 2020.

Yang, R., Sun, X., and Narasimhan, K. A generalized algorithm for multi-objective reinforcement learning and policy adaptation. *Advances in Neural Information Processing Systems*, 32, 2019.

Yang, Y., Zhou, T., Pechenizkiy, M., and Fang, M. Preference controllable reinforcement learning with advanced multi-objective optimization. In *Forty-second International Conference on Machine Learning*, 2025. URL https://openreview.net/forum?id=49g4c8MWHy.

Ye, M. and Liu, Q. Pareto navigation gradient descent: A first-order algorithm for optimization in Pareto set. In *Uncertainty in Artificial Intelligence*, pp. 2246–2255. PMLR, 2022.

Yuan, Y., Zheng, Z., Dong, Z., and HAO, J. MODULI: Unlocking preference generalization via diffusion models for offline multi-objective reinforcement learning. In *Forty-second International Conference on Machine Learning*, 2025. URL https://openreview.net/forum?id=V364YjXm3T.

Zhang, R. and Golovin, D. Random hypervolume scalarizations for provable multi-objective black box optimization. In *International Conference on Machine Learning*, pp. 11096–11105. PMLR, 2020.

Zhu, B., Dang, M., and Grover, A. Scaling Pareto-efficient decision making via offline multi-objective RL. In *The Eleventh International Conference on Learning Representations*, 2023. URL https://openreview.net/forum?id=Ki4ocDm364.

Zintgraf, L. M., Kanters, T. V., Roijers, D. M., Oliehoek, F., and Beau, P. Quality assessment of MORL algorithms: A utility-based approach. In *Benelearn 2015: Proceedings of the 24th Annual Machine Learning Conference of Belgium and the Netherlands*, 2015.

Zitzler, E. and Thiele, L. Multiobjective evolutionary algorithms: A comparative case study and the strength Pareto approach. *IEEE Transactions on Evolutionary Computation*, 3(4):257–271, 2002.

A. Algorithm

Algorithm 1 LLE-MORL (General d-Objective Case)

Require: Initial scalarization weights $\{w_k\}_{k=1}^{K}$ evenly spanning the preference space, Directional retraining weights $\{w_k^{(i)}\}_{k=1,i=1}^{K,m}$, Initialization training length T_{init}, Directional retraining length T_{dir}, Fine-tuning length T_{ref}, Step-scale factors $\alpha_{\text{start}}, \alpha_{\text{end}}, \Delta\alpha$

Ensure: Approximate Pareto-optimal policy set Π

1: $\Pi \leftarrow \emptyset$
2: $m \leftarrow d - 1$
3: $M \leftarrow \left\lfloor \frac{\alpha_{\text{end}} - \alpha_{\text{start}}}{\Delta\alpha} \right\rfloor + 1$
4:
5: **Initialization:**
6: **for** $k = 1$ to K **do**
7:      Train base policy θ_{w_k} with PPO under weight w_k for T_{init} steps
8: **end for**
9:
10: **Directional Retraining:**
11: **for** $k = 1$ to $K - 1$ **do**
12:      **for** $i = 1$ to m **do**
13:          $\theta_k^{(i)} \leftarrow$ continue training θ_{w_k} under $w_k^{(i)}$ for T_{dir} steps
14:          $\Delta\theta_k^{(i)} \leftarrow \theta_k^{(i)} - \theta_{w_k}$
15:          $\Delta w_k^{(i)} \leftarrow w_k^{(i)} - w_k$
16:      **end for**
17: **end for**
18:
19: **Locally Linear Extension:**
20: $\mathcal{C} \leftarrow \emptyset$
21: **for** $k = 1$ to K **do**
22:      **for all** combination of α_i on the grid $[\alpha_{\text{start}}, \alpha_{\text{end}}, \Delta\alpha]$ **do**
23:          $\theta_{k,\text{cand}} \leftarrow \theta_{w_k} + \sum_{i=1}^{m} \alpha_i \, \Delta\theta_k^{(i)}$
24:          $w_{k,\text{cand}} \leftarrow w_k + \sum_{i=1}^{m} \alpha_i \, \Delta w_k^{(i)}$
25:          Evaluate multi-objective performance $V(\theta_{k,\text{cand}})$ under weight $w_{k,\text{cand}}$
26:          $\mathcal{C} \leftarrow \mathcal{C} \cup \{(\theta_{k,\text{cand}}, w_{k,\text{cand}})\}$
27:      **end for**
28: **end for**
29:
30: **Candidate Selection:**
31: $\mathcal{N} \leftarrow$ non-dominated subset of $\mathcal{C}$
32:
33: **Preference-Aligned Fine-Tuning:**
34: $\mathcal{F} \leftarrow \emptyset$
35: **for all** $(\theta, w) \in \mathcal{N}$ **do**
36:      fine-tune θ for T_{ref} steps under w, yielding θ'
37:      add (θ', w) to $\mathcal{F}$
38: **end for**
39: $\mathcal{C}_{\text{all}} \leftarrow \mathcal{N} \cup \mathcal{F}$
40: $\mathcal{N}_{\text{final}} \leftarrow$ non-dominated subset of $\mathcal{C}_{\text{all}}$
41: $\Pi \leftarrow \Pi \cup \{\theta \mid (\theta, \cdot) \in \mathcal{N}_{\text{final}}\}$
42:
43: **return** Π

In this section, we present a complete description of LLE-MORL, an efficient procedure for tracing an approximate Pareto front in a d-objective setting. Algorithm 1 details this process.

The core pipeline involves several stages. First, K base policies $\{\theta_{w_k}\}$ are trained, each under its respective initial weight w_k for T_{init} steps. Next, for each base policy θ_{w_k}, we perform directional retraining to obtain $m = d - 1$ local directions: continuing training under nearby preferences $w_k^{(i)}$ for T_{dir} steps yields directional policies $\theta_k^{(i)}$, from which we compute the parameter updates $\Delta\theta_k^{(i)} = \theta_k^{(i)} - \theta_{w_k}$ and preference shifts $\Delta w_k^{(i)} = w_k^{(i)} - w_k$. In the Locally Linear Extension stage, we generate a candidate set $\mathcal{C}$ by combining these directions with step-scale factors $\{\alpha_i\}$ chosen from a grid $[\alpha_{\text{start}}, \alpha_{\text{end}}]$ with step size $\Delta\alpha$, producing up to M^m candidates per base policy together with matched weights $w_{k,\text{cand}}$. We then select the non-dominated subset $\mathcal{N} \subset \mathcal{C}$ and apply Preference-Aligned Fine-Tuning for T_{ref} steps to obtain refined policies $\mathcal{F}$. Finally, LLE-MORL returns Π, the non-dominated set extracted from $\mathcal{N} \cup \mathcal{F}$, which forms the final approximate Pareto front.

B. Theoretical Analysis

Throughout, $\|\cdot\|$ denotes the Euclidean norm on vectors by default, other norms on matrices are defined explicitly.

Definition B.1. Parameter-Performance Relationship (PPR). Let $\Theta \subseteq \mathbb{R}^n$ be the space of policy parameters, and V be the expected discounted return as a function $V : \Theta \to \mathbb{R}^d$ of the parameter θ. We say that V exhibits a *parameter–performance relationship* on an open region $U \subseteq \Theta$ if $\exists \delta > 0$ and a function $h : U \times B_\delta(0) \to \mathbb{R}^d$, *s.t.* $\forall \theta \in U$ and perturbation $\Delta\theta$ satisfying $\|\Delta\theta\| < \delta$ and $\theta + \Delta\theta \in U$, the difference in the performance space is:

$$V(\theta + \Delta\theta) \; - \; V(\theta) \; = \; h\big(\theta, \Delta\theta\big). \tag{4}$$

To clarify when LLE-MORL can reliably reconstruct a Pareto front, we present the theoretical analysis here. We consider here the Pareto fronts P that are differentiable manifolds, meaning that it is locally similar to Euclidean space and derivatives can be defined. As a slight generalisation, we can assume that the Pareto front is a non-connected manifold or a set of manifolds, including zero-dimensional manifolds (discrete points) or sets of manifolds of different dimensions. We will not further discuss this generalization apart from mentioning the fact that it is possible to reach all components and to produce sufficiently many charts of each of the components of the Pareto front. For the theoretical framework, we propose the following assumptions:

Assumption B.2. (Manifold Assumption) The Pareto front P is a set of differentiable manifold branches embedded in the performance space, which consist of all non-dominated points.

Assumption B.3. (Continuity of PPR function h) The function h in definition 3.1 is Lipschitz continuous with respect to the second variable $\Delta\theta$.

Remark on Assumption B.3: This assumption can be reduced to more basic conditions on the expected discount return V, where V is associated to the training phase through PPO algorithm. Such reduction is implemented by Theorem B.4.

Theorem B.4. *(Continuity of PPR function h, corresponding to Theorem 3.2) Denote the expected discounted return by $V : U \to \mathbb{R}^d$ where $U \subseteq \Theta \subseteq \mathbb{R}^n$ is an open set. There are two groups of sufficient conditions for Lipschitz continuity of $h(\theta, \Delta\theta)$ with respect to the second variable $\Delta\theta$:*

(i) $V \in \mathbb{C}^1(U)$ and $\forall a \in \mathcal{A}, s \in \mathcal{S}$

$$\sup_{\theta \in U} \big\| \nabla_\theta \log \pi_\theta(a|s) \big\| \le \mathcal{G} < \infty, \tag{5}$$

the inequality states that the score function (Baxter & Bartlett, 2001) is bounded by constant $\mathcal{G}$. This is a common assumption in the related researches (Aydin & Eksin, 2023; Shi et al., 2024).

Proof: (i) For a fixed parameter $\theta \in U$, define $h_\theta(\Delta) := V(\theta + \Delta) - V(\theta)$. Suppose the objective return is:

$$V(\theta) = \mathbb{E}_{\pi_\theta}\left[\sum_{t=0}^{\infty} \gamma^t \boldsymbol{r}(s_t, a_t) \right] \in \mathbb{R}^d, \tag{6}$$

with bounded rewards $\|\boldsymbol{r}(s,a)\| \le \mathcal{R}$, and $\pi_\theta(a|s)$ is a differentiable stochastic policy such that the score function $\nabla_\theta \log \pi_\theta(a|s)$ (Baxter & Bartlett, 2001) is locally bounded on a neighbourhood U of θ, i.e. Equation 5. Further, denote $\boldsymbol{d}(\tau) := \sum_{t=0}^{\infty} \gamma^t \boldsymbol{r}(s_t, a_t)$, where τ is state-action trajectory $(s_0, a_0, s_1, a_1, ...)$.

Next, take the gradient of V about θ and make transformations:

$$\nabla_\theta V(\theta) = \nabla_\theta \mathbb{E}_{\pi_\theta} \left[\sum_{t=0}^\infty \gamma^t \boldsymbol{r}(s_t, a_t) \right] \tag{7}$$

$$= \nabla_\theta \int \boldsymbol{d}(\tau) p_\theta(\tau) d\tau \tag{8}$$

$$= \int \boldsymbol{d}(\tau) \cdot \nabla_\theta p_\theta(\tau) d\tau \tag{9}$$

$$= \int \boldsymbol{d}(\tau) \cdot p_\theta(\tau) \nabla_\theta \log p_\theta(\tau) d\tau \tag{10}$$

$$= \mathbb{E}_{\pi_\theta} [\boldsymbol{d}(\tau) \nabla_\theta \log p_\theta(\tau)] \tag{11}$$

$$= \mathbb{E}_{\pi_\theta} \left[\sum_{t=0}^\infty \gamma^t \boldsymbol{r}(s_t, a_t) \sum_{k=0}^\infty \nabla_\theta \log \pi_\theta(a_k \mid s_k) \right] \tag{12}$$

$$= \mathbb{E}_{\pi_\theta} \left[\sum_{t=0}^\infty \gamma^t \boldsymbol{r}(s_t, a_t) \sum_{k=0}^t \nabla_\theta \log \pi_\theta(a_k | s_k) \right]. \tag{13}$$

The last equality follows from the standard causality rearrangement in the policy gradient theorem, where future score terms do not affect past returns. Above boundedness conditions on $\boldsymbol{r}$ and score function implies a uniform bound of $\nabla_\theta V$:

$$\|\nabla_\theta V(\theta)\| \leq \sum_{t=0}^\infty \gamma^t \mathcal{R}(t+1)\mathcal{G} = \frac{\mathcal{R}\mathcal{G}}{(1-\gamma)^2}. \tag{14}$$

Hence V is locally Lipschitz on U. Further, let $L_V := \sup_{\theta \in U} \|\nabla_\theta V(\theta)\| \leq \frac{\mathcal{R}\mathcal{G}}{(1-\gamma)^2}$, we have:

$$\|h_\theta(\Delta_1) - h_\theta(\Delta_2)\| = \|V(\theta + \Delta_1) - V(\theta + \Delta_2)\| \leq L_V \|\Delta_1 - \Delta_2\|. \tag{15}$$

Hence $h_\theta(\Delta) = h(\theta, \Delta)$ is Lipschitz on the ball $\Delta \in B_\delta(0)$ with $\theta + B_\delta(0) \subset U$: In particular, Assumption B.3 holds with Lipschitz constant $L_h \leq L_V \leq R_{\max} G/(1-\gamma)^2$ under local C^1 regularity of V and bounded score function conditions.

Theorem B.4 derives the Lipschitz continuity of PPR function h. Hence, small perturbations in the policy parameters only induce controllable small changes in the multi-objective performance vector V. In particular, along any path in the parameter space contained in the neighbour $\theta + B_\delta(0)$ of a fixed θ, the image under $V : \Theta \to \mathbb{R}^d$ varies continuously and bounded. This property is significant in reconstructing the Pareto surface produced by LLE algorithm: with a suitable small stepsize, expanded policy candidates map to a controlled neighborhood of the performance from initialisation. This guarantee is embodied and verified in the empirical results shown in Figure 3. Theorem B.4 serves as one of the theoretical foundations that guarantees the performance of the central algorithm is stable in approximating and constructing the Pareto front.

Corollary B.5. *(Surface continuity guaranteed by Lipschitz PPR) Algorithm LLE can always generate a continuous surface in the performance space, as an approximation to Pareto front, given appropriate regularity conditions and range of α.*

Proof: Suppose Theorem B.4 holds at a fixed θ, i.e., $\exists \delta, L_V > 0$ such that for all Δ_1, Δ_2 with $\|\Delta_1\|, \|\Delta_2\| \leq \delta$, we have:

$$\|V(\theta + \Delta_1) - V(\theta + \Delta_2)\| \leq L_V \|\Delta_1 - \Delta_2\|.$$

Then for any two parameters $\theta_1, \theta_2 \in \theta + B_\delta(0)$, if $\|V(\theta_1) - V(\theta_2)\| \geq \varepsilon > 0$, we have $\|\theta_1 - \theta_2\| \geq \varepsilon/L$. In particular, within the PPR neighbourhood $\theta + B_\delta(0)$, solutions that are separated obviously in the performance space must correspond to separated policies set in the parameter space, so LLE with sufficiently small step size cannot induce a spurious large displacement in performance space.

Remark that this corollary can not give us information whether the surface constructed is or closed to the Pareto front.

Corollary B.6. *(Lipschitz continuity of V) If Theorem B.4 holds, then $V(\theta)$ is also Lipschitz continuous for $\theta \in U \subseteq \Theta$.*

Assumption B.7. (Initialization) The initialization in Algorithm 1 stated in Section 3.4 identifies K different points on the optimal Pareto front. Thus, we have at least one accurate initial point for each branch of Pareto front.

Proof: $\forall \theta_1, \theta_2 \in U \subseteq \Theta$, in Equation 15, substitute $\theta = \theta_2$, $\Delta_1 = \theta_1 - \theta_2$, $\Delta_2 = 0$. Then we immediately have:

$$\|V(\theta_1) - V(\theta_2)\| \leq L_V \|\theta_1 - \theta_2\|. \tag{16}$$

Thus, $V(\theta)$ is Lipschitz continuous with constant L_V.

Condition B.8. (Chart of Pareto manifold) Based on Assumption B.2, $\mathcal{P} \in \mathcal{M}^m(\mathbb{R}^d)$, where the dimension of $\mathcal{P}$ is $m = d - 1$, and $\forall v \in \mathcal{P}$ is non-dominated. By definition, $\forall v \in \mathcal{P}$, there exists an open neighbourhood $P_v \subset \mathcal{P}$ and a chart:

$$\varphi_v : P_v \to \Omega_v \subset \mathbb{R}^{d-1} \tag{17}$$

where Ω_v is an open set, without loss of generality, we choose the chart such that $\varphi_v(v) = 0$. And φ_v is a C^k diffeomorphism ($k \geq 1$), with the inverse mapping is denoted by: $\varphi_v^{-1} : \Omega_v \to P_v \subset \mathbb{R}^d$.

Condition B.9. (Local lifting of a Pareto neighbourhood) Based on Condition B.8, Consider a fixed $v \in \mathcal{P}$ and its open neighbourhood $P_v \subset \mathcal{P}$. Suppose a corresponding policy parameter θ_v satisfying $V(\theta_v) = v$. Define an equivalence relation $\sim$ on Θ by $\theta_1 \sim \theta_2$ if $V(\theta_1) = V(\theta_2)$, and denote the quotient space by $\Theta/\sim$. Assume there exist $\Theta_v \subset \Theta$ consisting of the representative elements of $\Theta/\sim$, satisfying the following conditions:

$(i) \ \exists \delta > 0, \ s.t. \ \Theta_v \subseteq B_\delta(\theta_v). \tag{18}$

$(ii) \ V[\Theta_v] = P_v. \tag{19}$

$(iii) \ \forall \theta \in \Theta_v, \ |\Theta_v \cap [\theta]| = 1. \tag{20}$

where $B_\delta(\theta_v)$ denote an open ball with radius δ centres on θ_v, $[\theta] \in \Theta/\sim$ represent the equivalence class of θ, and $|\cdot|$ denote the cardinality of set. By (ii), we have $V|_{\Theta_v} : \Theta_v \twoheadrightarrow P_v$ is a surjection. By (iii), we have $V|_{\Theta_v} : \Theta_v \hookrightarrow P_v$ is an injection. Therefore, there is a bijection between Θ_v and P_v, denoted by $V|_{\Theta_v} : \Theta_v \to P_v$.

Condition B.9 serves two purposes. Firstly, the localization $\Theta_v \subset B_\delta(\theta_v)$ and $V(\Theta_v) = P_v$ ensures that the entire Pareto neighborhood P_v can be lifted to a region in parameter space, so the algorithm does not need to traverse distant solution components. This is the prerequisite under which local linear extrapolation in parameter space is meaningful for approximating the same Pareto branch. Second, the representative constraint $|\Theta_v \cap [\theta]| = 1$ removes the multi-to-one ambiguity of V by selecting exactly one representative from each equivalence class, so that notions such as parameter proximity, difference directions, and extrapolation updates are well-defined on the lifted set. More specifically, it formulates an injection from Θ_v to the Pareto neighborhood of v. Without this condition, a single performance could correspond to many distant parameters and retrained $\Delta\theta$ directions would be unstable and unreliable in exploring the Pareto front.

Figure 5. Manifold Map between Pareto front manifold and its local lifting. With each initialization $\theta^{(0)}$, we denote its performance v and the neighbour on the Pareto front manifold to be P_v. Based on our assumption and conditions, the local lifting, i.e. Θ_v is also a manifold of the same dimension of P_v, located in the neighbourhood of $\theta^{(0)}$. The Linear extrapolation corresponds to the approximation of the tangent space of Θ_v. Each time, LLE-MORL reconstruct the Pareto front branch where v is located. With the appropriate choices of initialization $\theta_k^{(0)}$, it reconstructs all of the branches where the corresponding $v_k = V(\theta_k^{(0)})$ is located.

Theorem B.10. *(Local lifting manifold, corresponding to Theorem 3.4) Let $P_v \subset \mathcal{P}$ be as in Condition B.8, where $P_v \in \mathcal{M}^m(\mathbb{R}^d)$ with a C^k chart $\varphi_v : P_v \to \Omega_v \subset \mathbb{R}^m$. Suppose $V|_{\Theta_v} : \Theta_v \to P_v$ is a bijection as in Condition B.9. If both $V|_{\Theta_v}$ and $(V|_{\Theta_v})^{-1}$ are C^k. i.e. ther is a diffeomorphism $V|_{\Theta_v} \in \mathrm{Diff}^k(\Theta_v, P_v)$. Then $\Theta_v \in \mathcal{M}^m(\mathbb{R}^n)$, with an C^k chart $\psi_v : \Theta_v \to \Omega_v \subset \mathbb{R}^m$.*

Proof: Fix a C^k chart $\varphi_v : P_v \to \Omega_v \subset \mathbb{R}^m$ from Condition B.8. Define $\psi_v := \varphi_v \circ V|_{\Theta_v} : \Theta_v \to \Omega_v$.

Since φ_v and $V|_{\Theta_v}$ are C^k, ψ_v is C^k, $\psi_v^{-1} := V|_{\Theta_v}^{-1} \circ \varphi_v^{-1} : \Omega_v \to \Theta_v$ is C^k because $V|_{\Theta_v}^{-1}$ and φ_v^{-1} are C^k.

Hence ψ_v is a C^k diffeomorphism between Θ_v and the open set $\Omega_v \subset \mathbb{R}^m$, which proves Θ_v is an m-dimensional C^k manifold embedded in $\mathbb{R}^n$, $\Theta_v \in \mathcal{M}^m(\mathbb{R}^n)$.

Condition B.11. *(Local extension directions, corresponding to Condition 3.5)* Fix $v \in \mathcal{P}$, an open neighbourhood $P_v \subset \mathcal{P}$ as in Condition B.8, and the corresponding lifted set $\Theta_v \subset \Theta$ from Condition B.9. Suppose the initialization returns $\theta^{(0)} \in \Theta_v$ with $V(\theta^{(0)}) = v$ by Assmption B.7. Applying $m = \dim \mathcal{P}$ distinct nearby preference perturbations and directional retraining from $\theta^{(0)}$, one obtains $\theta^{(i)} \in \Theta_v$, $i = 1, \ldots, m$, such that

$$\mathcal{D} := \left[\theta^{(1)} - \theta^{(0)}, \ \theta^{(2)} - \theta^{(0)}, \ \ldots, \ \theta^{(m)} - \theta^{(0)}\right] \in \mathbb{R}^{n \times m} \tag{21}$$

has full column rank, i.e. $\mathrm{rank}(\mathcal{D}) = m$. Further, $\mathrm{span}(\mathcal{D})$ provides an approximation to the tangent space of Θ_v at $\theta^{(0)}$, i.e. $T_{\theta^{(0)}}\Theta_v$ under Theorem B.10. This explains Step (2) in the Algorithm 1 stated in Section 3.4.

Lemma B.12. *(Coordinates of linear extension and error matrix) Let ψ_v be as in Theorem B.10, without loss of generality, define $\psi_v(\theta^{(0)}) = 0$, and denote $x^{(i)} := \psi_v(\theta^{(i)})$ and $X := [x^{(1)}, \ldots, x^{(m)}] \in \mathbb{R}^{m \times m}$. Let $\mathcal{J} := D\psi_v^{-1}(0)$ be the Jacobian at the origin of ψ_v^{-1}, and suppose ψ_v^{-1} is C^2 with $\|D^2(\psi_v^{-1})(x)\| \leq \eta$ on the neighbourhood of 0. Define $\mathcal{D}$ as in Condition B.11. Then there exists error matrix $E \in \mathbb{R}^{n \times m}$ such that: $\mathcal{D} = \mathcal{J}X + E$ and its L_2 norm is controlled by:*

$$\|E\|_2 \leq \frac{\eta}{2}\sqrt{m} \max_{1 \leq i \leq m} \|x^{(i)}\|^2. \tag{22}$$

Let $\sigma_{\min}(\mathcal{D})$ be the smallest singular value of $\mathcal{D}$, i.e. $\sigma_{\min}(\mathcal{D}) := \inf_{\|x\|=1} \|\mathcal{D}x\|_2$. If $\|E\|_2 < \sigma_{\min}(\mathcal{D})$, then X is invertible.

proof: (I). Apply Taylor expansion of ψ_v^{-1} at 0, where $\psi_v^{-1}(0) = \theta^{(0)}$:

$$\psi_v^{-1}(x^{(i)}) = \psi_v^{-1}(0) + \mathcal{J}x^{(i)} + r^{(i)} \tag{23}$$

where $r^{(i)}$ are remainder of the second order. Equivalently,

$$\theta^{(i)} - \theta^{(0)} = \mathcal{J}x^{(i)} + r^{(i)} \tag{24}$$

Arrange all formulas of $1 \leq i \leq m$ in matrix form, we have:

$$\mathcal{D} = \mathcal{J}X + E \tag{25}$$

Matrix $E := \left[r^{(1)}, r^{(2)}, \ldots, r^{(m)}\right] \in \mathbb{R}^{n \times m}$ is named error matrix as it gives the error of linear approximation. Matrix X is the coordinates map of manifold $\Theta_v \in \mathcal{M}^m(\mathbb{R}^n)$ with respect to the linear extension $\theta^{(i)}$.

Next, we derive the upper bound of E. Denote the components of $\psi_v^{-1} = \left[\psi_1^{-1}, \ldots, \psi_n^{-1}\right]$ with $\psi_\ell^{-1} : \Omega_v \subset \mathbb{R}^m \to \mathbb{R}$. For $x \in \Omega_v$ and $u, w \in \mathbb{R}^m$, define the second derivative as a bilinear map (operator on u, w pair):

$$D^2(\psi_v^{-1})(x)[u, w] := \left[u^\top \nabla^2 \psi_1^{-1}(x) \, w, \ \ldots, \ u^\top \nabla^2 \psi_n^{-1}(x) \, w\right]^\top \in \mathbb{R}^n, \tag{26}$$

where $\nabla^2 \psi_\ell^{-1}(x) = \left[\frac{\partial^2 \psi_\ell^{-1}}{\partial x_i \partial x_j}(x)\right]_{i,j=1}^m$ is the Hessian of ψ_ℓ^{-1}. Accordingly, define the operator norm:

$$\|D^2(\psi_v^{-1})(x)\| := \sup_{u,w \neq 0} \frac{\|D^2(\psi_v^{-1})(x)[u, w]\|_2}{\|u\| \cdot \|w\|} \tag{27}$$

By Taylor's theorem, with the notation above, the reminder of ψ_v^{-1}, i.e. $r^{(i)}$ has a explicit integral form:

$$\psi_v^{-1}(x^{(i)}) = \psi_v^{-1}(0) + \mathcal{J}x^{(i)} + \int_0^1 (1-t)D^2(\psi_v^{-1})(tx^{(i)})[x^{(i)}, x^{(i)}]dt \tag{28}$$

Thus,

$$\|r^{(i)}\| \leq \int_0^1 (1-t) \, \|D^2(\psi_v^{-1})(tx^{(i)})[x^{(i)}, x^{(i)}]\| \, dt \leq \int_0^1 (1-t) \, \eta \|x^{(i)}\|^2 \, dt = \frac{\eta}{2}\|x^{(i)}\|^2. \tag{29}$$

Then we can control the norm of E, i.e. Equation 22, by the upper bound of its Frobenius norm $\|E\|_F$:

$$\|E\|_2 \leq \|E\|_F = \Big(\sum_{i=1}^m \|r^{(i)}\|^2\Big)^{1/2} \leq \frac{\eta}{2}\Big(\sum_{i=1}^m \|x^{(i)}\|^4\Big)^{1/2} \leq \frac{\eta}{2}\sqrt{m} \max_{1\leq i\leq m} \|x^{(i)}\|^2. \tag{30}$$

(II). If X were singular, there would exist $u \in \mathbb{R}^m$, $u \neq 0$ with $Xu = 0$, hence $\mathcal{D}u = Eu$. Therefore

$$\|\mathcal{D}u\| \leq \|E\|_2 \cdot \|u\|. \tag{31}$$

On the other hand, by definition of $\sigma_{\min}(\mathcal{D})$,

$$\|\mathcal{D}u\| = \|u\| \cdot \Big\|\mathcal{D}\frac{u}{\|u\|}\Big\| \geq \|u\| \cdot \inf_{\|x\|=1} \|\mathcal{D}x\|_2 \geq \sigma_{\min}(\mathcal{D}) \, \|u\|. \tag{32}$$

Thus $\sigma_{\min}(\mathcal{D}) \leq \|E\|_2$, contradicting $\|E\|_2 < \sigma_{\min}(\mathcal{D})$. Therefore X is invertible.

All above, the preparation work is finished. We now focus on the core theorem supporting the effectiveness of LLE algorithm. Notations in the previous conditions and theorems are continuously adopted:

Theorem B.13. *(Local Pareto error of LLE, corresponding to Theorem 3.6) Denote the Linear exploration by $\tilde{\theta}(\alpha) := \theta^{(0)} + \mathcal{D}\alpha$. Then for a suitable range of $\alpha \in \mathbb{R}^m$ with $X\alpha \in \Omega_v$, the error of exploration to the actual Pareto front is controlled by:*

$$\mathrm{dist}\big(V(\tilde{\theta}(\alpha)), \mathcal{P}_v\big) \leq \frac{L_V \eta}{2} \cdot \max_{1\leq i\leq m} \|x^{(i)}\|^2 \cdot \Big(\sqrt{m}\,\|\alpha\| + m\,\|\alpha\|^2\Big). \tag{33}$$

Proof: Define the point-to-set distance in performance space by

$$\mathrm{dist}(z, \mathcal{P}_v) := \inf_{p\in\mathcal{P}_v} \|z - p\|, \qquad z \in \mathbb{R}^d. \tag{34}$$

Let $\psi_v : \Theta_v \to \Omega_v$ be the C^2 chart from Theorem B.10 with $\psi_v(\theta^{(0)}) = 0$ and set $\theta^\star(\alpha) := \psi_v^{-1}(X\alpha) \in \Theta_v$, which is the lifted manifold point with chart coordinate $X\alpha$. Since $V[\Theta_v] = \mathcal{P}_v$, we have $V(\theta^\star(\alpha)) \in \mathcal{P}_v$ whenever $X\alpha \in \Omega_v$. Hence,

$$\mathrm{dist}\big(V(\tilde{\theta}(\alpha)), \mathcal{P}_v\big) \leq \big\|V(\tilde{\theta}(\alpha)) - V(\theta^\star(\alpha))\big\|_2. \tag{35}$$

By the local Lipschitz continuity of V on the neighbourhood under consideration,

$$\big\|V(\tilde{\theta}(\alpha)) - V(\theta^\star(\alpha))\big\|_2 \leq L_V \big\|\tilde{\theta}(\alpha) - \theta^\star(\alpha)\big\|_2. \tag{36}$$

It remains to bound $\|\tilde{\theta}(\alpha) - \theta^\star(\alpha)\|_2$. By Lemma B.12, for the retraining points $\theta^{(i)} \in \Theta_v$ we have $\mathcal{D} = \mathcal{J}X + E$ with $\mathcal{J} := D(\psi_v^{-1})(0)$. By Taylor's theorem with integral remainder applied to ψ_v^{-1},

$$\psi_v^{-1}(X\alpha) = \psi_v^{-1}(0) + \mathcal{J}(X\alpha) + r(X\alpha) \tag{37}$$

By Equation 29, $\|r(X\alpha)\| \leq \frac{\eta}{2}\|X\alpha\|^2$. Using $\psi_v^{-1}(0) = \theta^{(0)}$ and $\tilde{\theta}(\alpha) = \theta^{(0)} + \mathcal{D}\alpha$, we obtain

$$\tilde{\theta}(\alpha) - \psi_v^{-1}(X\alpha) = \Big(\theta^{(0)} + \mathcal{D}\alpha\Big) - \Big(\theta^{(0)} + \mathcal{J}X\alpha + r(X\alpha)\Big) = E\alpha - r(X\alpha). \tag{38}$$

Therefore,

$$\big\|\tilde{\theta}(\alpha) - \theta^\star(\alpha)\big\| = \big\|E\alpha - r(X\alpha)\big\| \leq \|E\|_2 \, \|\alpha\| + \frac{\eta}{2}\|X\alpha\|^2. \tag{39}$$

Combining inequalities of Equation 39, 35, 36, yields:

$$\mathrm{dist}\big(V(\tilde{\theta}(\alpha)), \mathcal{P}_v\big) \leq L_V\Big(\|E\|_2 \cdot \|\alpha\| + \frac{\eta}{2}\|X\alpha\|^2\Big) \tag{40}$$

17

Further, let $\| \cdot \|_F$ be Frobenius norm,

$$\|X\alpha\|^2 \leq \|X\|_2^2 \cdot \|\alpha\|^2 \leq \|X\|_F^2 \cdot \|\alpha\|^2 = \|\alpha\|^2 \cdot \sum_{i=1}^{m} \|x^{(i)}\|^2 \leq m\|\alpha\|^2 \cdot \max_{1 \leq i \leq m} \|x^{(i)}\|^2 \tag{41}$$

Substitute Equation 22 from Lemma B.12, Equation 41 into Equation 40, we have :

$$\text{dist}\big(V(\tilde{\theta}(\alpha)), \mathcal{P}_v\big) \leq \frac{L_V \eta}{2} \cdot \max_{1 \leq i \leq m} \|x^{(i)}\|^2 \cdot \Big(\sqrt{m}\, \|\alpha\| + m\, \|\alpha\|^2\Big), \tag{42}$$

which completes the proof.

Under the conditions of the theorem, we describe the LLE-MORL time complexity as follows.

Proposition B.14. *(Time complexity) Given that the number of objectives is n, the number of base policies is K, the base policy training time is T, the number of locally linear extensions sampled per direction is M, and noting that the locally linear extension is training-free, the expected running time of LLE-MORL is $O(TK + KM^{n-1})$.*

Proof for proposition B.14. In an n-objective reinforcement learning problem, if the Pareto front in the policy parameter space can be represented as a differentiable $(n-1)$-dimensional manifold, LLE-MORL can locally reconstruct this manifold by extending each base policy along $(n-1)$ distinct directions obtained via directional retraining. The locally linear extension then combines these directions to generate a grid of new candidate policies. In a n-objective task, $n-1$ directional retrained directions are used to form a $(n-1)$-dimensional grid: $\theta = \theta_{\text{base}} + \sum \alpha_i(\theta_i - \theta_{\text{base}})$, $i = 1, \ldots, n-1$, allowing dense coverage of the local Pareto surface with or without further training. Training K base policies requires $O(TK)$. Around each base policy, local linear extension samples M^{n-1} candidate policies across the $n-1$-dimensional tangent space. These extensions require no retraining, so their cost is dominated by evaluation, yielding the second term $O(KM^{n-1})$. Thus the overall runtime is $O(TK + KM^{n-1})$.

The first term in the time complexity proposition corresponds to the cost of training K base policies, which is the dominant cost. The second term accounts for generating and evaluating M^{n-1} extended policies per base policy. This step is training-free and its cost is controllable via $M = (\frac{\alpha_{\max} - \alpha_{\min}}{\Delta \alpha})$, allowing the user to balance Pareto front accuracy/density against computational resources. The second term grows exponentially with the number of objectives, but for low- to moderate-dimensional objectives, this cost remains small compared to policy training. For very high-dimensional objective spaces, adaptive sampling or sparse grids can mitigate this cost.

C. Experiment Setup Details

C.1. Benchmarks

To evaluate the performance of our proposed LLE-MORL method and compare it against existing baselines, we utilise a suite of continuous control benchmarks from the MO-Gymnasium library (Felten et al., 2023). These environments are designed to test the ability of an agent to learn policies that effectively balance multiple, often conflicting objectives. The specific environments and their multi-objective reward formulations are detailed below:

MO-SWIMMER-V5. A planar, three-link swimmer operating in a viscous fluid, utilising a 2D continuous action space to control its joint torques. The objectives are to maximise forward velocity along the x-axis and minimise the control cost.

The observation space $\mathcal{S} \subset \mathbb{R}^8$ includes joint angles and velocities, and the action space $\mathcal{A} \subset \mathbb{R}^2$ represents joint torques in $[-1, 1]$. Let x_{before} and x_{after} be the x-coordinates of the centre of mass of swimmer before and after an action, Δt be the time step, and a_j be the j-th component of the action vector.

The first objective is the forward speed

$$R_1 = \frac{x_{\text{after}} - x_{\text{before}}}{\Delta t},$$

and the second objective is the energy efficiency (negative control cost):

$$R_2 = -\sum_{j} a_j^2$$

MO-HOPPER-2OBJ-V5. This environment features a 2D one-legged hopper with a 3-dimensional continuous action space controlling torques for its thigh, leg, and foot joints. Originally a 3-objective task (forward speed, jump height, control cost), we use the 2-objective variant, in which the separate control-cost objective is added to other objectives.

The observation space $\mathcal{S} \subset \mathbb{R}^{11}$ includes joint states and torso position, and the action space $\mathcal{A} \subset \mathbb{R}^3$ represents joint torques in $[-1, 1]$. Let $v_x = (x_{\text{after}} - x_{\text{before}})/\Delta t$ be the forward velocity of the agent along the x-axis, where x_{after} and x_{before} are x-positions of the torso. Let $h_{\text{jump}} = 10 \times (z_{\text{after}} - z_{\text{init}})$ be a measure of jumping height, where z_{after} is the current z-position of the torso and z_{init} is its initial z-position. Let c_{ctrl} be the positive control cost, computed as $w_{\text{env\_ctrl}} \sum_j (a_j)^2$, where $w_{\text{env\_ctrl}}$ is the environment control cost weight (typically 0.001). Let r_{healthy} be the health reward (typically $+1$ if the agent has not fallen). The reward vector $\mathbf{R} = [R_1, R_2]$ is defined as:

- R_1 (Adjusted Forward Performance):

$$R_1 = v_x + r_{\text{healthy}} - c_{\text{ctrl}}$$

- R_2 (Adjusted Height Performance):

$$R_2 = h_{\text{jump}} + r_{\text{healthy}} - c_{\text{ctrl}}$$

MO-ANT-2OBJ-V5. A quadrupedal "ant" robot in 2D with an eight-dimensional action space for joint torques. By default, the environment emits a three-dimensional reward vector: (1) x-velocity, (2) y-velocity, and (3) control cost. Here, we use the two-objective variant in which the separate control-cost objective is added to other objectives.

The observation space $\mathcal{S} \subset \mathbb{R}^{27}$ includes joint states, torso position, and contact forces, and the action space $\mathcal{A} \subset \mathbb{R}^8$ represents joint torques in $[-1, 1]$. Let $v_x = (x_{\text{after}} - x_{\text{before}})/\Delta t$ be the forward velocity of the agent along the x-axis, where x_{after} and x_{before} are x-positions of the torso. Let $v_y = (y_{\text{after}} - y_{\text{before}})/\Delta t$ be the forward velocity of the agent along the y-axis, where y_{after} and y_{before} are y-positions of the torso. Let c_{ctrl} be the positive control cost, computed as $w_{\text{env\_ctrl}} \sum_j (a_j)^2$, where $w_{\text{env\_ctrl}}$ is the environment control cost weight (typically 0.05). Let r_{healthy} be the health reward (typically $+1$ if the Ant is healthy). Let p_{contact} be the positive contact penalty, which is used for penalising the Ant if the external contact forces are too large, computed as $w_{\text{env\_contact}} \sum_k (\text{force}_k)^2$, where $w_{\text{env\_contact}}$ is the environment contact cost weight (typically 5×10^{-4}). The reward vector $\mathbf{R} = [R_1, R_2]$ is defined as:

- R_1 (Adjusted x-Velocity Performance):

$$R_1 = v_x + r_{\text{healthy}} - c_{\text{ctrl}} - p_{\text{contact}}$$

- R_2 (Adjusted y-Velocity Performance):

$$R_2 = v_y + r_{\text{healthy}} - c_{\text{ctrl}} - p_{\text{contact}}$$

MO-HOPPER-3OBJ-V5. This environment is identical to MO-HOPPER-2OBJ-V5 in terms of state and action spaces, but retains all three original objectives instead of merging the control cost into the other rewards. As a result, the task features three objectives: forward speed, jump height, and control cost. The reward vector $\mathbf{R} = [R_1, R_2, R_3]$ is defined as:

- R_1 (x-Velocity Performance):

$$R_1 = v_x + r_{\text{healthy}}$$

- R_2 (y-Velocity Performance):

$$R_2 = h_{\text{jump}} + r_{\text{healthy}}$$

- R_3 (Control Cost):

$$R_3 = -c_{\text{ctrl}} + r_{\text{healthy}}$$

MO-ANT-3OBJ-V5. This environment is identical to MO-ANT-2OBJ-V5 in terms of state and action spaces, but retains all three original objectives instead of merging the control cost into the other rewards. As a result, the task features three objectives: x-velocity, y-velocity, and control cost. The reward vector $\mathbf{R} = [R_1, R_2, R_3]$ is defined as:

- R_1 (x-Velocity Performance):

$$R_1 = v_x + r_\text{healthy} - p_\text{contact}$$

- R_2 (y-Velocity Performance):

$$R_2 = v_y + r_\text{healthy} - p_\text{contact}$$

- R_3 (Control Cost):

$$R_3 = -c_\text{ctrl} + r_\text{healthy} - p_\text{contact}$$

C.2. Evaluation Metrics

We evaluate the quality of the approximate Pareto front using three standard metrics, following the formalism in (Zitzler & Thiele, 2002; Zintgraf et al., 2015; Hayes et al., 2022).

Hypervolume (HV). Let P be an approximate Pareto front and G_0 a reference point dominated by all $p \in P$. The hypervolume is $\mathcal{H}(P) = \int_{\mathbb{R}^d} \mathbb{1}_{H(P)}(z)\,dz$, where $H(P) = \{\, z \in \mathbb{R}^n \mid \exists j,\ 1 \le j \le |P| \ :\ G_0 \preceq z \preceq P(j)\}$. Here, $P(j)$ is the jth solution in P, the symbol $\preceq$ denotes objective dominance, and $\mathbb{1}_{H(P)}$ is an indicator function that equals 1 if $z \in H(P)$ and 0 otherwise. A higher hypervolume implies a front closer to and more extensive with respect to the true Pareto front.

Expected Utility (EU). Let P be an approximate Pareto front and Π be the corresponding policy set. The expected utility metric is $\mathcal{U}(P) = \mathbb{E}_{\omega \sim \Omega}\left[\max_{\pi \in \Pi}\ \omega^\top G_\omega^\pi\right]$. A higher EU denotes better average performance over preferences.

Sparsity (SP). Let P be an approximate Pareto front in a d-dimensional objective space. The sparsity metric is $S(P) = \frac{1}{|P|-1} \sum_{i=1}^{d} \sum_{k=1}^{|P|-1} \big(\tilde{G}_i(k) - \tilde{G}_i(k+1)\big)^2$, where $\tilde{G}_i$ is the sorted list of the ith objective values in P, and $\tilde{G}_i(k)$ is the kth entry in this sorted list. Lower sparsity indicates a more uniform distribution of solutions along each objective.

C.3. Hungarian matching distance

To measure structural similarity between policies, we use the Hungarian matching distance (Kuhn, 1955; Munkres, 1957).

Definition C.1. Hungarian matching distance. For a given layer l with neuron sets $A^{(l)}$ and $B^{(l)}$, let $w_i^{(l)}$ and $w_j^{(l)}$ denote the incoming weight vectors of neurons $i \in A^{(l)}$ and $j \in B^{(l)}$, respectively. The minimum-cost perfect matching $M^{(l)}$ between $A^{(l)}$ and $B^{(l)}$ is obtained by using the Hungarian algorithm:

$$M^{(l)} = \underset{\text{matching}}{\arg\min} \sum_{(i,j) \in \text{matching}} \left\| w_i^{(l)} - w_j^{(l)} \right\|_2 \tag{43}$$

The Hungarian matching distance between the two networks is then defined as

$$d_\text{Hungarian}(A, B) = \sum_{l=1}^{L} \sum_{(i,j) \in M^{(l)}} \left\| w_i^{(l)} - w_j^{(l)} \right\|_2 \tag{44}$$

where L is the total number of layers.

C.4. Sanity Check Details

In Section 3.2, the sanity check was designed as a qualitative validation of the parameter–performance relationship (PPR), rather than a full experiment.

To construct policy pairs, we trained 11 base policies $\theta_{\omega 1}$ using the scalarization vector ω_1 that were equally distributed in the preference space, i.e. $\omega_1 = [1, 0], [0.9, 0.1], ..., [0, 1]$.

For each base policy, we formed a paired scalarization vector ω_2 by shifting ω_1 with a retraining shift parameter δ_s:

$$\omega_2 = \begin{cases} [\omega_{11} - \delta_s, \omega_{12} + \delta_s], \text{ if } \omega_{11} - \delta_s \in [0,1] \\\\ [\omega_{11} + \delta_s, \omega_{12} - \delta_s], \text{ otherwise} \end{cases} \quad (45)$$

where $\delta_s \in \{0.1, 0.2, 0.3, 0.4, 0.5\}$. This procedure yielded multiple pairs of (ω_1, ω_2) across the preference space. For each pair, we performed short retraining from θ_{ω_1} under ω_2 and compared the orignial θ_{ω_1} and resulting model $\theta_{\omega'}$ with the independently trained θ_{ω_2}. This allowed us to consistently observe that retrained policies stay close in parameter space (low Hungarian distance), while having directional movement in performance space, supporting the local PPR hypothesis. Figure 2 in the main paper presents a representative example from these trials.

C.5. Training Details

All learning phases within our LLE-MORL algorithm, including the initial training of base policies, the directional retraining, and the final preference-aligned fine-tuning, utilize the Proximal Policy Optimization (PPO) algorithm (Schulman et al., 2017). We employed a standard PPO implementation from the Stable Baselines3 library (Raffin et al., 2019). The PPO parameters used across all training stages and benchmarks are detailed in Table 3.

The specific parameters for the LLE-MORL pipeline include:

- **Number of Initial Base Policies** (K): The total count of base policies θ_{w_k}, trained in the initialization stage. The corresponding K initial scalarization weights $\{w_k\}_{k=1}^K$ are generated by evenly distributing them across the preference space (e.g., for 2D objectives, from $[1,0]$ to $[0,1]$ in K steps).

- **Initialization Training Timesteps** (T_{init}): The number of environment interaction steps for which the initial base policy θ_{w_k} is trained under its weight w_k.

- **Retraining Preference Shift Strategy (controlled by shift magnitude δ_s)**: Target scalarization weights $\{w_k^{(i)}\}$ for directional retraining are generated by shifting each initial weight w_k to a nearby, distinct point on the preference space. The extent of this shift is controlled by a hyperparameter δ_s.

- **Directional Retraining Timesteps** (T_{dir}): The number of environment interaction steps for which the base policy θ_{w_k} is retrained under its target weight w_k^i to produce $\theta_{w_k^{(i)}}$.

- **Step-Scale Factor Generation** ($\alpha_{\text{start}}, \alpha_{\text{end}}, \Delta\alpha$): The set of step-scale factors $\{\alpha_i\}$ used in Locally Linear Extension is generated based on a starting value (α_{start}), an ending value (α_{end}), and either a step increment ($\Delta\alpha$).

- **Fine-tuning Timesteps** (T_{ref}): The number of environment interaction steps for which the selected candidate policy from the extension phase is fine-tuned under its matched preference weight $w_{k,\text{cand}}$.

Table 3. PPO hyperparameters for benchmarks.

Parameter Name	MO-Swimmer	MO-Hopper-2d	MO-Ant-2d	MO-Hopper-3d	MO-Ant-3d
steps per actor batch	512	512	512	512	512
learning rate ($\times 10^{-4}$)	3	3	3	3	3
learning rate decay ratio	1	1	1	1	1
γ	0.995	0.995	0.995	0.995	0.995
GAE lambda	0.95	0.95	0.95	0.95	0.95
number of mini batches	32	32	32	32	32
PPO epochs	10	10	10	10	10
entropy coefficient	0.0	0.0	0.0	0.0	0.0
value loss coefficient	0.5	0.5	0.5	0.5	0.5
maximum gradient norm	0.5	0.5	0.5	0.5	0.5
clip parameter	0.2	0.2	0.2	0.2	0.2

In all experiments reported in the main results, we fix the number of initial base policies to $K = 6$, the retraining preference shift magnitude to $\delta_s = 0.1$, and the step-scale factor grid to $\alpha \in [-1.5, 1.5]$ with step size $\Delta\alpha = 0.05$. We need to clarify

Table 4. Approximate execution times (hours) for each method and benchmark under different settings.

(a) 2D sample-efficient setting

Method	MO-Swimmer	MO-Hopper-2d	MO-Ant-2d
GPI-LS	3	3	3
CAPQL	3	3	3
Q-Pensieve	3	3	3
MORL/D	1	1	1
LLE-MORL	1	1	1

(b) 2D standard-training setting

Method	MO-Swimmer	MO-Hopper-2d	MO-Ant-2d
GPI-LS	22	23	19
CAPQL	11	11	12
Q-Pensieve	17	15	18
MORL/D	3	3	3
LLE-MORL	3	3	3

(c) 3D setting

Method	MO-Hopper-3d	MO-Ant-3d
GPI-LS	44	43
CAPQL	13	18
Q-Pensieve	24	23
MORL/D	5	6
LLE-MORL	5	5

that K and δ_s are chosen for simplicity and are not intended to be optimal. We have an additional discussion about the choice of δ_s in Appendix D.1. The step-scale factor α controls the Locally Linear Extension stage and has a meaningful but limited influence on performance; its impact and selection are discussed in Appendix D.2.

For baseline methods, since the original papers do not evaluate performance on the same benchmark problems considered in this work, we adopt the implementations and hyperparameter settings provided by morl-baselines (Felten et al., 2023). As LLE-MORL is a PPO-based algorithm, we employ PPO hyperparameter configurations commonly used in PPO-based MORL methods, such as PGMORL (Xu et al., 2020), which serves as a standard and widely adopted reference for PPO settings in MORL tasks.

In all experiments reported in the main results, we strictly control the total training interaction budget for all methods to ensure a fair comparison. For LLE-MORL, this fixed budget is automatically partitioned across the three learning phases using a simple $3 : 1 : 1$ ratio for initial base policy training, directional retraining, and preference-aligned fine-tuning, respectively. When the total training budget is sufficiently large, allocating additional interaction steps to the base policy training stage can further improve performance, as directional retraining and fine-tuning require fewer updates. The optimal budget allocation depends on the target application and can be adjusted on a case-by-case basis.

C.6. Computational Resources

All experiments were run on a workstation equipped with an AMD Ryzen Threadripper PRO 5975WX (32 cores), an NVIDIA GeForce RTX 3090 GPU (24 GB GDDR6X), and 256 GiB of RAM, running Ubuntu 24.04 LTS. The software stack included CUDA Toolkit 12.0 and the corresponding NVIDIA drivers. Approximate execution times for all methods and benchmarks are reported separately in Table 4.

D. Additional Results

D.1. Effect of Directional Retraining Shift

This ablation study investigates the influence of the directional retraining shift δ_s, on the Locally Linear Extension process. We analyse the performance of the LLE-MORL-0 variant (which excludes fine-tuning) under the standard-training setting. We vary δ_s over the set $\{0.1, 0.2, 0.3, 0.4, 0.5\}$, keeping other parameters at their default values, and report Hypervolume (HV), Expected Utility (EU), and Sparsity (SP) for each environment in Table 5.

The results indicate that δ_s influences the resulting Pareto front approximation, as different shift values generate distinct extension trajectories that directly shape the front. While optimal performance varies across environments, a moderate retraining shift (e.g., δ_s in the range of 0.2 to 0.3, depending on the specific benchmark characteristics evident in Table 5) generally appears to strike an effective balance between front coverage (HV, EU) and solution diversity (SP). Our default configuration utilized $\delta_s = 0.1$, chosen for its simplicity and promising results in preliminary tests. However, this ablation

Table 5. Impact of retraining shift δ_s on LLE-MORL-0 performance (HV, EU, SP) under standard-training setting.

Environment	Metric	$\delta_s = 0.1$	$\delta_s = 0.2$	$\delta_s = 0.3$	$\delta_s = 0.4$	$\delta_s = 0.5$
MO-Swimmer	$HV(10^4)$	7.37	7.38	7.38	7.36	7.37
	$EU(10^1)$	1.03	1.29	1.41	0.99	1.60
	$SP(10^2)$	2.10	0.83	3.05	2.39	2.12
MO-Hopper-2d	$HV(10^5)$	4.88	4.84	4.79	4.86	4.80
	$EU(10^2)$	5.65	5.56	5.49	5.54	5.58
	$SP(10^2)$	7.20	4.49	3.33	2.54	3.33
MO-Ant-2d	$HV(10^5)$	2.43	2.66	2.65	2.72	2.44
	$EU(10^2)$	3.44	3.94	3.69	3.95	3.66
	$SP(10^3)$	1.76	2.64	2.23	8.98	2.41

Table 6. Influence of Step-Scale α on LLE-MORL-0 performance under standard-training setting.

Environment	Metric	$(\alpha_{start}, \alpha_{end})$	(-1,1)				(-1.5,1.5)				(-2,2)				(-3,3)			
		$\Delta\alpha$	0.01	0.05	0.1	0.5	0.01	0.05	0.1	0.5	0.01	0.05	0.1	0.5	0.01	0.05	0.1	0.5
MO-Swimmer	$HV(10^4)$		7.37	7.37	7.37	7.33	7.38	7.37	7.37	7.33	7.40	7.40	7.39	7.34	7.40	7.40	7.40	7.34
	$EU(10^1)$		1.08	1.27	1.32	1.33	1.08	1.03	1.42	1.65	1.13	1.41	1.53	1.70	1.43	1.75	1.73	2.37
	$SP(10^2)$		0.24	1.17	2.54	25.55	1.13	2.10	1.46	25.55	0.11	0.53	1.18	11.48	0.11	0.51	1.18	11.48
MO-Hopper-2d	$HV(10^5)$		4.95	4.88	4.85	4.80	4.96	4.88	4.90	4.80	4.95	4.88	4.88	4.81	4.96	4.88	4.88	4.81
	$EU(10^2)$		5.82	5.74	5.73	5.75	5.76	5.65	5.72	5.75	5.75	5.69	5.69	5.67	5.75	5.69	5.69	5.68
	$SP(10^2)$		5.63	9.43	11.58	60.35	5.01	7.20	13.06	60.35	3.02	5.42	10.05	29.66	3.62	5.41	10.05	29.66
MO-Ant-2d	$HV(10^5)$		2.57	2.43	2.40	2.23	2.60	2.43	2.23	2.14	2.60	2.47	2.25	2.14	2.60	2.47	2.25	2.14
	$EU(10^2)$		3.61	3.47	3.62	3.66	3.66	3.44	3.44	3.31	3.67	3.59	3.43	3.37	3.67	3.59	3.43	3.37
	$SP(10^3)$		0.54	2.03	3.11	7.92	1.85	1.76	1.79	8.36	1.85	1.55	1.79	8.36	1.85	1.55	1.79	8.36

demonstrates that this typical shift is not universally optimal; selecting an appropriately tuned moderate δ_s can further enhance the quality and coverage of the extended manifold, thereby improving the final Pareto front approximation achieved by LLE-MORL-0.

D.2. Effect of Step-Scale in Locally Linear Extension

We next examine how the choice of step-scale factors $\{\alpha_j\}$ — defined by their start α_{start}, end α_{end}, and increment $\Delta\alpha$ — influences the performance of LLE-MORL-0. For each benchmark, we compare different ranges and resolutions of $\{\alpha_j\}$ and report HV, EU, and SP in Table 6.

The choice of $\Delta\alpha$ significantly impacts Sparsity (SP), as shown in Table 6. Finer increments (smaller $\Delta\alpha$) lead to substantially lower SP values, indicating denser Pareto front approximations, whereas coarser steps result in sparser solutions. This confirms that LLE offers a training-free mechanism to control the density of the approximated front simply by adjusting $\Delta\alpha$.

Regarding the range of α_j (controlled by α_{start} and α_{end}), expanding it generally leads to improvements in both HV and EU, as the extension manifold can reach further from the initial policy along the identified directional vector (visualized conceptually in Figure 3). However, Table 6 suggests that an extremely wide range does not always yield proportional gains in coverage. This indicates that beyond a certain point, the linearity assumption underpinning LLE may become less effective for extending the front into novel, high-quality regions using a single directional vector, or that the most valuable regions reachable by the current $\Delta\theta$ vectors are already sufficiently captured.

E. Discussion on Reliability and Robustness

In the LLE-MORL algorithmic procedure, the underlying Reinforcement Learning method (PPO) used in the training and retraining phases is subject to inherent stochasticity arising from factors such as random seed initialisation for neural network weights and data sampling during training. This means that while the overarching behaviour and effectiveness of LLE-MORL are generally reproducible, the exact set of policies discovered on the approximated Pareto front, their specific parameter values, or their ordering might exhibit some variation across independent runs started with different random seeds. Consequently, direct averaging of entire Pareto fronts or performing straightforward statistical tests on the precise composition of these policy sets can be non-trivial and may not always be the most informative way to capture the consistent

ability of the algorithm to find high-quality solution regions.

Our demonstration of reliability and robustness relies on: (1) the consistent observation of the superior performance of LLE-MORL in generating high-quality Pareto fronts compared to baselines; (2) sensitivity analyses of key hyperparameters (detailed in Appendix D), which show consistent outcome patterns within certain parameter ranges; (3) the qualitative consistency in the shape, extent, and dominance characteristics of the visualized Pareto fronts (e.g. Figure 4); and (4) the quantitative results reported in Table 1 and Table 2 across multiple seeds, further reinforcing the statistical reliability of our findings. These combined observations support the robustness of our conclusions and the effectiveness of LLE-MORL.

F. Limitations

Limitations of our approach are implied by inherent challenges in multi-objective optimisation, but we also note some limitations that are specific to our algorithm and require further study.

- A larger number of objectives is a problem for most of the existing MORL algorithms. Although usually some of the objectives are of different importance and can be lexicographically ranked, so that the complexity does not necessarily increase exponentially with the number of objectives. The high-dimensional case is nevertheless challenging, but our approach can be seen as promising: In higher dimensions, the number of solutions that are in the same local quasi-linear patch increases dramatically, so that the efficiency of the proposed local search will be even more beneficial. This benefit could be reduced by the potentially increasing complexity of the topological relation between the performance space and the parameter space which could be a fascinating subject for future work.

- We are assuming that the Pareto front consists of a limited number of connectivity components which have a manifold structure. While there is no theoretical bound to the complexity of the Pareto front, the idea of MORL implies that the objectives are at least in some sense comparable. For Pareto fronts that are fractal or of high genus, the result of multi-objective optimisation lacks robustness, although it will neither be possible to fix any limits for the complexity of the Pareto front. However, as long as there are only a limited number of manifold-like connectivity components, our algorithm will be applicable.

- Widely different scales and elasticities of the objectives can lead to problems as in optimisation in anisotropic error landscapes. Step size control that helps in gradient methods in optimisation will also be useful here, but has not been studied yet, as the typical (benchmark) problems are sufficiently isotropic.

- The density of the identified solutions on the Pareto front is clearly a challenge, which may be solved by step size control as mentioned in the previous point. This concerns higher-dimensional cases as well as extended one-dimensional trails as visible in the top trail in Figure 3c also a simple reduction of the parameter $\Delta\alpha$ at the observation of large steps in the performance space could have solved this issue already so that a more uniform covering of the Pareto from is not difficult to achieve in the present approach. See also Appendix D.2. In contrast to other approaches, locally smooth regions of the Pareto front can trivially be tracked by LLE-MORL. Concave regions connected to the Pareto front will be followed through without problem, but will need to be removed in a single postprocessing step as they are dominated by other solutions. Even full patches of solutions may turn out to be Pareto sub-optimal and require a similar treatment.

- We have made use of scalarisation to seed the solution domains, whereas the reconstruction of the Pareto front is done by a lateral process that does not depend on preference weights. It is in principle possible that a solution patch is not reachable by any scalarisation-based seeding attempt, see also the early discussion in (Vamplew et al., 2008). In this case our approach might not find this patch, although it is still possible that it is found by retraining from a different solution domain as shown in Figure 3c.